ARMY RESEARCH LABORATORY

Recent Applications of CFD to the Aerodynamics of Army Projectiles

Walter B. Sturek
Charles J. Nietubicz
Jubaraj Sahu
Paul Weinacht

ARL-TR-22 December 1992

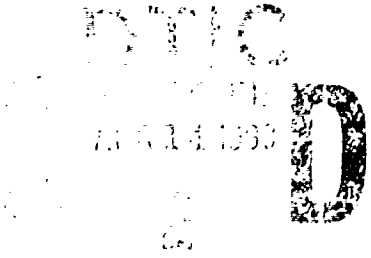

NOTICES

Destroy this report when it is no longer needed. DO NOT return it to the originator.

Additional copies of this report may be obtained from the National Technical Information Service, U.S. Department of Commerce, 5285 Port Royal Road, Springfield, VA 22161.

The findings of this report are not to be construed as an official Department of the Army position, unless so designated by other authorized documents.

The use of trade names or manufacturers' names in this report does not constitute indorsement of any commercial product.

REPORT DOCUMENTATION PAGE

Form Approved
OMB No. 0704-0188

1. AGENCY USE ONLY (Leave blank)	2. REPORT DATE	3. REPORT TYPE AND DATES COVERED
	December 1992	Final, Jan 89 - Sep 92

4. TITLE AND SUBTITLE
Recent Applications of CFD to the Aerodynamics of Army Projectiles

5. FUNDING NUMBERS
611102A-00-001 AJ

6. AUTHOR(S)
Walter B. Sturek, Charles J. Nietubicz, Jubaraj Sahu, and Paul Weinacht

7. PERFORMING ORGANIZATION NAME(S) AND ADDRESS(ES)
U.S. Army Research Laboratory
ATTN: AMSRL-CI-CA
Aberdeen Proving Ground, MD 21005-5066

8. PERFORMING ORGANIZATION REPORT NUMBER

9. SPONSORING / MONITORING AGENCY NAME(S) AND ADDRESS(ES)
U.S. Army Research Laboratory
ATTN: AMSRL-OP-CI-B (Tech Lib)
Aberdeen Proving Ground, MD 21005-5066

10. SPONSORING / MONITORING AGENCY REPORT NUMBER
ARL-TR-22

11. SUPPLEMENTARY NOTES
The report supersedes BRL-IMR-973, September 1992.

12a. DISTRIBUTION / AVAILABILITY STATEMENT
Approved for public release; distribution is unlimited.

12b. DISTRIBUTION CODE

13. ABSTRACT *(Maximum 200 words)*

The ability to predict the complete set of aerodynamic performance parameters for projectile configurations has been a stated goal of the Computational Aerodynamics Branch, U.S. Army Ballistic Research Laboratory. In order to achieve this goal, predictive capabilities which utilize Navier-Stokes computational techniques have been developed and applied to an extensive number of projectile configurations. A summary of code validation efforts and applications for both spin stabilized and fin stabilized projectile configurations are described. Significant progress in the predictive capability for projectile aerodynamics has been achieved through the availability of substantial supercomputer resources and modern computational techniques. Current and future research areas of interest are described and provide an indication of computer resources and code enhancements needed to continue the progress in projectile computational aerodynamics.

14. SUBJECT TERMS
projectile aerodynamics; transonic flow; finned projectile aerodynamics; supersonic flow; turbulent boundary layer

15. NUMBER OF PAGES
56

16. PRICE CODE

17. SECURITY CLASSIFICATION OF REPORT	18. SECURITY CLASSIFICATION OF THIS PAGE	19. SECURITY CLASSIFICATION OF ABSTRACT	20. LIMITATION OF ABSTRACT
UNCLASSIFIED	UNCLASSIFIED	UNCLASSIFIED	UL

INTENTIONALLY LEFT BLANK.

ACKNOWLEDGEMENT

The results presented represent the efforts of several engineers and support personnel in the Computational Aerodynamics Branch of the Launch and Flight Division of the U.S. Army Ballistic Research Laboratory. In particular, the efforts of Mr. Edge, Mrs. Heavey, and Ms. Smith deserve special recognition.

INTENTIONALLY LEFT BLANK.

TABLE OF CONTENTS

LIST OF FIGURES

INTENTIONALLY LEFT BLANK.

1. INTRODUCTION

The objectives of this report are to: provide a summary of recent computational aerodynamic efforts at the U.S. Army Ballistic Research Laboratory (BRL), now reorganized as part of the newly formed U.S. Army Research Laboratory (ARL); provide an assessment of the current Computational Fluid Dynamics (CFD) capabilities as applied to Army shell; and indicate high priority research areas for further development of the predictive technology.

This report is the third summary discussion of CFD code validation and application to projectile aerodynamics. The first paper[1] reported the status of initial efforts to apply time-marching and space-marching techniques to bodies of revolution at transonic and supersonic velocities during the period 1978–1983. The second paper[2] reported similar efforts during the period 1983–1985 and also included some initial results for modeling of fin stabilized shell. The results emphasized here are relatively recent. They consist of examples of code validation, where the computational results were compared to established experimental data, and application, where the codes were used to predict the performance of proposed projectile designs.

2. CODES

The computational codes employed at the ARL for projectile aerodynamics emphasize Reynolds averaged Navier-Stokes techniques. Turbulent, viscous boundary-layer development plays a significant role in the development of important aerodynamic coefficients such as Magnus, drag, and roll damping. Thus, in order to avoid the requirement to apply multiple techniques to predict a complete set of aerodynamic performance factors, emphasis is placed on the application of the Reynolds averaged Navier-Stokes technique.

The techniques employed have been described extensively in the literature so no detailed descriptions will be provided here. Instead, a general overview of the computational codes employed and appropriate references will be provided. The techniques employed can be categorized as time-marching and space-marching.

The time-marching technique is used in the F3D code.[3] This technique, developed by Steger[3], is a flux-split, upwind scheme in the axial (main flow) direction and central differenced in the circumferential and normal direction. The F3D code provides a capability to partition the flow field into zonal regions or blocks to accommodate complex projectiles. Since the code is time-marching, it can be applied to predict subsonic and supersonic flow fields. Thus, this technique is required where regions of subsonic flow exist, such as: the base region of shell; local flow field separation; and for free-stream subsonic conditions. An earlier time-marching code, which has been used to perform base flow computations including mass injection in the base region, is an extension of the Azimuthal-Invariant code.[4] This code is fully implicit, centrally differenced and uses the approximate factorization of Beam-Warming.[5] Projectile spin is allowed through the Azimuthal-Invariant assumptions.

The space-marching technique is known as the PNS method. The code being used was originally developed by Schiff and Steger,[6] and has been extensively developed and refined by Rai and Chaussee.[7,8] This code also employs the Beam-Warming linearized block, approximately factored, numerical algorithm.[5] The space-marching feature results in highly efficient use of computational resources but restricts the application to supersonic free-stream conditions in which no separation in the streamwise flow occurs. This technique has proven to be highly useful in design applications for long L/D fin stabilized projectiles which fly at high supersonic speeds and small angles of attack.

3. GRID GENERATION

Army projectile shapes are generally simple bodies of revolution; and a combination of elliptic, hyperbolic, and algebraic grid generator codes are utilized to develop the computational grids. Grid generation for the time-marching codes is carried out using either algebraic[9] or hyperbolic[10] methods. Recently, an interactive hyperbolic grid generator was developed.[11] Projectiles with irregular base region configurations and with irregular fin geometries are becoming of increasing importance. With these added complexities, the grid generation process can become lengthy and cumbersome. Grid generation for the space-marching code is carried out algebraically for the cylindrical portion of the projectile. An elliptic technique[8] is used for generating the computational grid about the fin.

4. TURBULENCE MODELING

Army projectiles have surface finishes which enhance the transition to turbulence and fly under high dynamic pressure conditions at relatively low altitudes. Thus, modeling the turbulent viscous layer is important for an accurate prediction of the aerodynamic forces. The Baldwin-Lomax algebraic turbulence model[12] is routinely used for the body surface. Simple extensions of this model[13] have been found to be beneficial for computing flows in large, separated regions such as the projectile wake region and flow downstream of steps or protuberances. A more advanced k-ε model has also been applied[14] with some success. Recent results using this model have been obtained and will be discussed later.

5. VALIDATION EXAMPLES

5.1 Spin-Stabilized Projectiles.

5.1.1 Pitch Damping at Supersonic Velocities. Pitch damping, according to linear theory,[15,16] is proportional to the side moment acting on a projectile undergoing a steady coning motion. This provides a convenient and efficient technique for predicting pitch damping using the PNS code in a rotating coordinate system. Thus, pitch damping can be predicted from a single computational sweep over the projectile body for a specified coning motion. Figure 1 shows a schematic illustration of the coning motion as applied here.

The prediction of pitch damping from a coning motion for bodies of revolution at supersonic velocities has been accomplished using the PNS code with modifications for centrifugal and Coriolis forces.[17] This technique has been applied to the Army-Navy Spinner Rocket (ANSR) configurations shown in Figure 2. Examples of predictions for pitch damping compared to free flight range tests for these shapes are shown in Figures 3 and 4. These results are in excellent agreement with the data and provide solid verification of the technique. Current emphasis is being placed on extension of the technique to the time-marching numerical code, F3D. This will provide prediction capability of pitch damping coefficients for projectiles at transonic velocities.

5.1.2 Static and Dynamic Coefficients at Transonic Velocities. The aerodynamics for a projectile with a boattail are known to experience a critical behavior at transonic velocities. This behavior has been shown to result from the longitudinally asymmetric shock location which occurs on the projectile at angle of attack as it traverses the transonic regime. In the previous review,[2] initial results of the computed longitudinal pressure distribution for the secant-ogive-cylinder-boattail configuration shown in Figure 5 were presented and shown to be in good agreement with the experimental data. At that time, only one Mach number had been computed using the F3D zonal code. Subsequent calculations have been performed[18] on the same configuration for a Mach number range of $0.9 \leq \text{Mach} \leq 1.2$ and compared with the experimental wind tunnel data.[19] A comparison is shown in Figure 6 between the computed wind and lee side pressure distributions and the experimental data for Mach = 1.1. The comparison is excellent and provides a sound basis for the critical behavior to be determined. The computed pitching moment coefficient shown in Figure 7 indicates the highly localized critical behavior of boattailed shell at transonic speeds. These results required a grid of $238 \times 39 \times 50$ points in the longitudinal, circumferential half plane, and normal direction, respectively, to adequately resolve the shock location and thus predict the critical behavior. The run time for each Mach number on the Cray 2 was approximately 25 hours.

A further test of the validation accuracy can be established by predictions of fielded Army shell. A series of computations[18] have been performed for the M549 configuration shown in Figure 8. The Mach number ranged from $0.7 \leq M_\infty \leq 1.5$ and all computations were performed at $\alpha = 2°$. A representative plot of the Mach contours is shown in Figure 9 for $M_\infty = 0.94$. The wind and lee side longitudinally asymmetric shock location is clearly evident on the boattail of the M549. The static aerodynamic coefficients have been obtained over the computed Mach number range. Figure 10 is a plot of the slope of the pitching moment coefficient comparing the computed results with the experimental data. The critical aerodynamic behavior computed is in generally good agreement with the experimental data. At most, the discrepancy is 5 to 7%, which is within the experimental accuracy of the flight data in the transonic regime.

A pacing item in projectile aerodynamics has been the accurate determination of the Magnus effect on a spinning projectile at transonic speeds. The Magnus effect results from a spin-induced distortion of the viscous boundary-layer which exists on a spinning shell at angle of attack. Since

this problem has no plane of symmetry, it is fully three dimensional and requires significant computer resources to achieve a solution. A unique experimental test was conducted by Miller and Molnar[20] in which surface pressures were measured on a spinning wind tunnel model. The model is shown in Figure 11. The tests were conducted for a Mach number of 0.94, at angles of attack of 0, 4, and 10 degrees, and for spin rates of 0 and 4,900 rpm. Computations using the F3D code were performed for this configuration at 4 and 10 degrees angle of attack.[21] The grid developed for this fully three dimensional problem consisted of three zones and required 82 million words of memory. The run time for each case on the Cray 2 was approximately 80 hours. A comparison between computational and experimental data is shown in Figure 12 for the Magnus force as it develops along the body. The pressure data has been integrated for the Magnus force and is represented by open circles and squares for four and ten degrees angle of attack, respectively. The solid and dashed lines are the computed results. An experimental result obtained from a wind tunnel force balance test[22] on the same configuration is plotted as closed symbols. The results for both the four and ten degree angle of attack cases are shown to be in good agreement with the force balance results. Although there is a discrepancy between the experimental measurements obtained using force balance and wall pressure technique as well as between the experiment and computations, the results are considered to be satisfactory given the small magnitude of the Magnus force. The computed Magnus force is in better agreement with the force balance data which is considered to be the more accurate of the two experimental results.

5.1.3 Base Flow Including Bleed and Jets. The ability to predict the base flow for shell is required for accurate determination of the projectile's total drag. The complete validation of base flow is generally quite difficult due in part to the lack of good experimental data and the uncertainty associated with applying turbulence models in the recirculating wake flow. Additional complexity is added when base bleed effects or base jets are included.

Recent tests have been conducted at the University of Illinois[23] on a cylindrical afterbody instrumented with a series of pressure taps. The model was mounted from the plenum chamber which provided an unobstructed wake flow. Both base pressure measurements and velocity measurements of the near wake were taken for a condition of Mach = 2.46 free stream flow. The data set, which includes profiles for u and v velocities, turbulent kinetic energy, and Reynolds

stress, represents a very complete set of code validation data. The F3D code, using a k-ε and two algebraic turbulence models, was applied to the experimental configuration.[24] The upstream boundary condition was obtained from the experimental profile. Figure 13 shows the computed base pressure using the different turbulence models compared to the experimental data. Both algebraic models are shown to predict a significant variation in base pressure in the radial direction. The k-ε model results are found to be almost constant and in good agreement with the data except near the base centerline.

Validation efforts for base bleed are still not complete; however, an indication of the current predictive capability can be obtained from the results of a study for the M864 base bleed configuration. The M864 is an Army shell which burns a solid propellant in the base region. Initial computations[25] were performed using the Azimuthal-Invariant base flow code. The mass injection was considered to be a perfect gas at 300 K, ranging from I = 0.005 to 0.02. The Mach number ranged from 0.8 to 3.0. Although direct comparison with data cannot be made, a plot is shown in Figure 14 which compares the computed results with a number of base bleed experiments.[26] The results are presented as $d(P_b/P_\infty)/dI$ vs. Mach number. The computed results are in general agreement with the experimental data base.

Afterbody flows containing a propulsive jet are also of interest and validation efforts have been under study.[2] The work described here is for an exhaust jet within an axisymmetric boattailed afterbody. The freestream Mach number is 2.0 with a jet exit of M = 2.5. The jet to free-stream pressure varied from 1 to 15. The conical nozzle has a half-angle of 20 degrees. Results showing the computed density contours compared with the experimental Schlieren photograph are shown in Figure 15 for the high pressure ratio case. Qualitative agreement can be seen in the comparison. A plot of the average base pressure as a function of exit pressure is shown in Figure 16. The agreement is good for the pressure ratio of 9 and 15 but falls off at the lower values. Additional validation efforts are required for jet interaction problems.

5.2 Fin Stabilized Projectiles. The M735 and M829 are long L/D, high velocity, finned projectiles for which extensive aerodynamics range test data are available for comparison with computational results. These projectiles are also of interest in that they represent a class of projectile for which developmental efforts are currently in progress. Thus, validation of

computational techniques for these projectiles provide assurance to the development community that predictions for proposed projectile concepts can be carried out with confidence. The results of computational studies to predict the aerodynamics of these projectiles are reported in Refs. 27 and 28.

The geometry of the M735 and M829 are shown in Figs. 17 and 18, respectively. Computational results for pitching moment coefficient are compared with firing data in Figures 19 and 20 for the M735 and M829, respectively. The computed results show the same trend with Mach number as the experimental data; however, the computed results are consistently higher, by about 5%, than the experimental data. This is likely the result of neglecting the sabot grooves in the computational model. Sabot grooves cause an increase in the thickness of the boundary layer. This thickened viscous layer would be expected to decrease the effectiveness of the fins, thus reducing the magnitude of the pitching moment. The pitching moment is very accurately determined in aerodynamics range tests and is an excellent coefficient to compare with computational results. However, the normal force is not so accurately determined experimentally due to the heavy mass of the long L/D projectiles. A comparison between computation and experiment for the normal force coefficient is shown in Figure 21 for the M735 projectile.

Since these finned projectiles are designed to fly with a slow spin rate to reduce dispersion, dynamic coefficients such as roll damping and pitch damping are of strong interest. The projectile fins typically have leading edge and trailing edge cuts and chamfers to induce specific amounts of spin. The capability to predict these effects is permitted through the incorporation of the effects of centrifugal and Coriolis forces into the PNS computational code. Examples of predictions for equilibrium spin rate, roll producing moment, and roll damping for the M829 projectile are shown in Figures 22, 23, and 24, respectively. In general, the computed results pass through the scatter in the experimental data. These particular coefficients are determined with considerable difficulty in free flight range tests. Thus, it is of particular interest to have a predictive capability for these dynamic coefficients.

The pitch damping, as discussed previously, is proportional to the side moment acting on a projectile undergoing a steady coning motion. This provides a convenient and efficient technique for predicting the pitch damping using the PNS code in a rotating coordinate system. Thus, the

pitch damping coefficient can be predicted from a single computational sweep over the projectile body for a specified coning motion. Examples of predicted results for pitch damping are compared to experimental data for the M735 and M829 projectiles in Figures 25 and 26, respectively. The computed results provide a consistent trend with Mach number and, in general, pass through the scatter in the experimental data. The experimental determination of pitch damping for these projectiles is poorly determined due to the heavy mass of the projectile and the small angle of attack flight. In order to achieve better determination of the pitch damping in range tests, projectiles with the same exterior shape but with different mass distributions can be tested.

5.3 Flare Stabilized Projectiles. A family of flare stabilized projectiles was studied recently through an experimental investigation in the ARL Aerodynamics Range.[29] These data have been compared to PNS computations in Refs. 30 and 31. The projectile geometries considered in this study are shown in Figures 27 and 28.

Comparisons of pitch damping for three projectile configurations as a function of Mach number are shown in Figures 29, 30, and 31. A summary of the pitch damping results for all configurations at Mach 4 is shown in Figure 32. These results indicate that the computational technique is capable of predicting the magnitude of the pitch damping within the experimental scatter and discriminating between the design variations.

6. APPLICATION EXAMPLES

The predictive capabilities have been applied recently to developmental problems in a truly predictive manner in that the computations were performed prior to the fabrication of hardware. The computational results provided aerodynamic flight performance information as a function of proposed design configuration and had significant influence on the configurations to be tested.

6.1 Scorpion Configuration. Computational support for the Scorpion project was initiated to evaluate the aerodynamic behavior of a proposed projectile concept. This concept involved a primary carrier or parent configuration with trailing cylindrical segments in the wake. A schematic of this concept is shown in Figure 33. Aerodynamics of the lead projectile as well as a

determination of the drag for the segments while in the wake of the parent projectile were of interest. Also, no known experimental or analytical data were available for this wake interaction problem.

6.1.1 Leading Projectile Aerodynamics. Computational aerodynamic predictions[32] were performed to determine an exterior shape to achieve optimum performance in terms of flight stability and spin rate. Three configurations for which computations have been performed are shown in Figure 34. Computational results which compare the pitching moments and pitch damping for variations of these configurations as a function of the sweep angle for the fins and strakes are shown in Figures 35 and 36, respectively. The pitch damping and moments of inertia properties of the projectiles enable the pitch damping behavior of candidate configurations to be computed. A comparison of the pitch damping motion of the original and optimized configurations is shown in Figure 37. The design of the straked flare was selected for the test projectile in order to achieve maximum damping of initial yaw and a specified spin rate at the test station. The spin rate was controlled through cant of the strakes and was determined by computations in the rotating coordinate frame. The flight tests indicated that the projectile performed in a highly satisfactory manner.

6.1.2 Trailing Segments and Trajectory. Multibody computations were performed[33] for the parent projectile with both one and two trailing segments at Mach = 4.4 and 0 degrees angle of attack. A series of results were obtained with the single segment configuration at various separation distances from the parent projectile. The computations were performed without considering the relative motion between parent and segment. Figure 38 shows a Mach number contour plot of the base region with the segment at 2 calibers (1 caliber is 1 parent body diameter) downstream of the base. The segment at this point is immersed within the low speed recirculation zone of the parent projectile. When the segment is at a position of 10 calibers (Figure 39), where the wake flow is now supersonic, a leading bow shock is seen in front of the segment. Of particular interest is the drag history for the segments which is presented in Figure 40. Results are shown for both one and two cylindrical segments in the wake. The drag is seen to increase as a function of separation distance for the single segment case. The multiple segment results show the decreased drag experienced by subsequent segments. The drag predictions provided valuable input to a point mass trajectory program which was used to

compute the flight history for multiple segments at various initial escape velocities. The results of the trajectory computation are shown in Figure 41. The separation distance between the base of the parent projectile and the leading segment was found to be 81 calibers (3.6 meters) after the parent projectile had traveled 100 meters. This computational study was found to be useful in the design of the segments and for setting up the experimental range tests.

6.2. Extend Rod. The Extend Rod project was established to evaluate a proposed projectile concept for which the projectile extends in flight after launch. Computational aerodynamic predictions were performed to determine the flare configuration to achieve the desired drag and flight stability of the projectile in the fully extended configuration.[34] The launch and extended projectile geometries are shown in Figure 42. The predicted pitch damping for candidate configurations as a function of flare angle is shown in Figure 43. The predicted pitch damping behavior is shown in Figure 44 for the launch and extended configurations of the selected geometry. It is of interest to note that the pitch damping of the extended configuration is less rapid than the launch configuration even though the pitch damping moment coefficient of the extended configuration is greater. This behavior is a result of the increased longitudinal moment of inertial of the extended configuration.

6.3 Projectiles with Base Cavities. The majority of previous base flow computations and analytical studies considered the base of a projectile to be a flat surface. This was true even though many of the actual projectile configurations have some form of a base cavity. General opinion had been that the internal base shape was of no consequence aerodynamically and would have little or no effect on the overall flight performance parameters. Range firings of the M825 and computations for the M865, both of which have base cavities, provided evidence that the base configuration can indeed affect the base flow and, in turn, have a significant effect on the aerodynamics.

6.3.1 M825 Projectile. The M825 originally had an aluminum/steel base which contained a flat (standard) cavity. As a result of a product improvement initiative, a new all steel base configuration was designed which contained a dome cavity. The base cavity configurations are shown in Figure 45. As a result of range tests, it was found that differences in the aerodynamic performance of the two bases existed. A computational study was performed[35] to predict these

differences and to further understand the fluid dynamic behavior. The computed normal force and pitching moment coefficients are shown in Figures 46 and 47, respectively. The computations clearly show a difference in the aerodynamics between the two configurations and are in general agreement with the trend of the experimental data. An evaluation of the computed velocity vectors indicated that the changes were due in part to a displacement of the shear layer near the base corner of the standard configuration which weakened the expansion at the base corner.

6.3.2 M865 Projectile. The M865 is a flare stabilized projectile which simulates the flight of long L/D finned projectiles for training purposes. The M865 contains a tracer in the base cavity. In firing tests, it was noticed that the tracer, which the gunner uses to detect the impact point of the round, was not visible for the full range of interest. In an effort to uncover a cause for this unsatisfactory performance, a computational study was carried out in which the pressure distribution in the wake of the projectile was computed. The computational study[36] was conducted for the velocity range of interest, $2.0 \leq M \leq 5.0$. Figure 48 shows the computational model of the M865 including the base region cavity. The computations did not consider any mass injection effects. An analysis of the base flow results indicated the presence of a pressure spike located along the axis near the base of the projectile. Figure 49 is a plot of the center line pressure extending from the interior cavity downstream. The jump in pressure can be seen for all Mach numbers with the largest spike occurring at $M = 3.0$. This rapid pressure change was considered as a potential reason for the premature tracer burnout. In an attempt to reduce or eliminate this problem a modified cavity design was proposed and computations were performed. The results, shown in Figure 50, are again in the form of centerline pressure for the $M = 3.0$ case. The comparison between the original and modified configuration shows that the original pressure spike has been reduced. This result has provided a potential cause for the unexpected behavior of the M865 projectile.

7. AERODYNAMIC HEATING

The stabilizing fins for long L/D KE penetrator projectiles are made of aluminum alloy. Since the melting temperature of aluminum is approximately 960 K, these fins are vulnerable to the effects of in-bore and aerodynamic heating. No direct experimental measurements of the heating rates or temperature response of these fins are available due to the difficult environment and thin

geometry of the fins. However, qualitative visual and photographic observations during flight tests, which reveal structural deficiencies such as altered platform shape and "burning" of the fins, are available to indicate that melt temperature is reached for these fins.

Several studies to model the in-bore and free flight aerodynamic heating for these fins have been performed.[37,38,39] A recent study[39] reports results in which a newly developed finite volume heat conduction code[38] was utilized to predict the benefit of protective coating materials for fins. The computations included the effect of retardation of the projectile in flight through time-dependent boundary conditions for convective heat transfer and recovery temperature based on the known flight trajectory. The convective heat transfer and recovery temperature boundary conditions were determined using PNS code results for the full projectile with fins. Examples of the results achieved are shown in Figures 51, 52, and 53. Temperature contours for a flight time of 2.0 seconds for the aluminum fin with standard aluminum oxide coating is shown in Figure 51 and for the same conditions with a fiber epoxy coating in Figure 52. The temperature at the leading edge of the fin at mid-span is shown in Figure 53 as a function of flight time for the two coating materials. The substantial benefit of the ablative coating is illustrated.

The effects of aerodynamic heating are becoming increasingly important as the Army considers the development of longer range artillery shell and increased launch velocities using electromagnetic and electrothermal launcher technologies.

8. RESEARCH AREAS

Although a highly sophisticated computational predictive capability for projectile aerodynamics currently exists, active research is being carried out to further develop and refine this predictive capability. In particular, techniques for combustion modeling, zonal modeling techniques, and optimization of numerical algorithms for efficient utilization of massively parallel computer architectures are of interest. Requirements for improved turbulence modeling are expected to become of critical importance in the near future in applications where significant regions of flow separation occur such as high angles of attack and for highly deflected guidance fins.

8.1 Combustion Modeling. Combustion modeling is of interest to predict the effects of the burning of solid propellants for base bleed and rocket assist projectiles. These concepts are utilized to achieve increased range for artillery projectiles, which is an area of current interest.

An initial attempt to obtain a combustion capability for base bleed projectiles was begun though a contract with Scientific Research Associates. The computational approach which has been used for this effort was developed by Giebling and Buggelin.[40] Several combustion models which would be applicable to the projectile base flow problem were evaluated. The code (CMINT) is based on the solution of the Navier-Stokes equations coupled with the species conservation and turbulence model equations. Injectant gas mixtures of H_2 and H_2/CO were considered and applied to a flat base projectile configuration. Computations were performed on a flat base M864 configuration for conditions without bleed, with hot air bleed, and with reacting H_2/CO injection. All computations were performed at Mach = 2.0 and 0 degrees angle of attack. A combustion model consisting of nine species and twelve reactions was used. Temperature contours are shown in Figures 54 and 55 for hot mass injection and combustion, respectively. The effect of the hot mass injection is seen to be confined very near the base while combustion affects the entire recirculation region. The net decrease in base drag when combustion is added was found to be approximately 20%.

8.2 Zonal Techniques. Techniques to subdivide the projectile flow field into zones for ease and convenience of grid generation for highly complex projectile configurations are being pursued. Improved techniques for specifying the zonal boundaries and boundary conditions are needed in order to reduce the time required to generate computational grids and to set up the flow field solver. Guided projectile configurations with deflected fins and gaps between the fin and projectile body represent a significant challenge. The wraparound fin projectile, Figure 56, is another example of a configuration which could benefit from improved zonal techniques. An example of a grid generated for a wraparound configuration[41] is shown in Figure 57. The time required set up this geometry for solution by a Navier-Stokes code exceeded 3 months. Clearly, there is room for improvement in the structure of the Navier-Stokes solver and the grid generation technique.

In an attempt to provide more efficient methods for complex projectile configurations, research is currently being conducted to apply overset or Chimera[42] technology to multibody problems with relative motion. An example of a multibody problem is the Scorpion project described earlier. This work is in its initial stage and involves using the F3D code combined with a domain decomposition code called DCL3D developed by Meakin.[43] The computational approach is completed by applying the computed aerodynamic loads to the multiple bodies and computing the trajectory. This determines the position of the moving bodies for the next time step of the flow solver. This approach has been applied[44] with success to the space shuttle store separation process.

8.3 Turbulence Modeling. The Baldwin-Lomax algebraic turbulence model and simple modifications of this model have been utilized with good success for many Army projectile applications. However, as the configurations become more complex and the angles of attack considered result in flow with significant regions of flow separation, more advanced turbulence models will be required. Current efforts include the application of k-ε modeling in the base region of shell. The proper wake turbulence model for flows with combustion taking place is currently unknown. Another challenging application is the prediction of flow in the wake of finned projectiles. The relatively thin, blunt trailing edges of these fins require modeling techniques to resolve the free shear layers downstream of the fins and in the wake region of the projectile base.

8.4 Massively Parallel Techniques. The solution of complex projectile applications such as guided configurations, projectiles with combustion taking place in the base region, and transonic flight at large angles of attack require computers with greater than 100 million words of memory and result in computation times of greater than 50 hours on a Cray 2 class CPU. In order for CFD to provide timely input to the projectile design process, several orders of magnitude increase in computer memory and processing speed are required. This will only be achieved through successful optimization of computational techniques for massively parallel computer architectures. Efforts to achieve this enhanced capability are of great interest.

9. CONCLUDING REMARKS

The applied computational projectile aerodynamic research described above represents a summary of recent experience at the U.S. Army Research Laboratory. It is believed that a highly productive capability currently exists to assist projectile designers achieve optimized aerodynamic configurations. This is particularly true for supersonic velocity flight for spin, fin, and flare stabilized projectiles. The predictive capabilities described have been applied to a wide variety of recent projectile development projects with considerable success.

Areas in which further development of the predictive technology is desirable have been outlined. Research is ongoing at the U.S. Army Research Laboratory to address these deficiencies; however, relevant research efforts in other government research institutions and academia are encouraged.

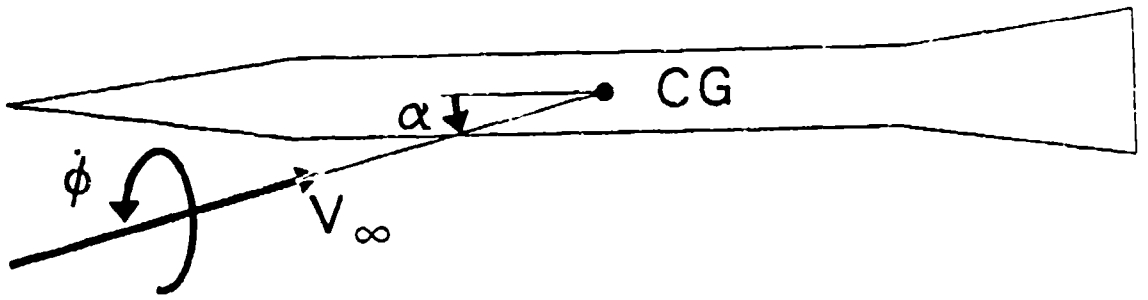

Figure 1. Schematic of coning motion

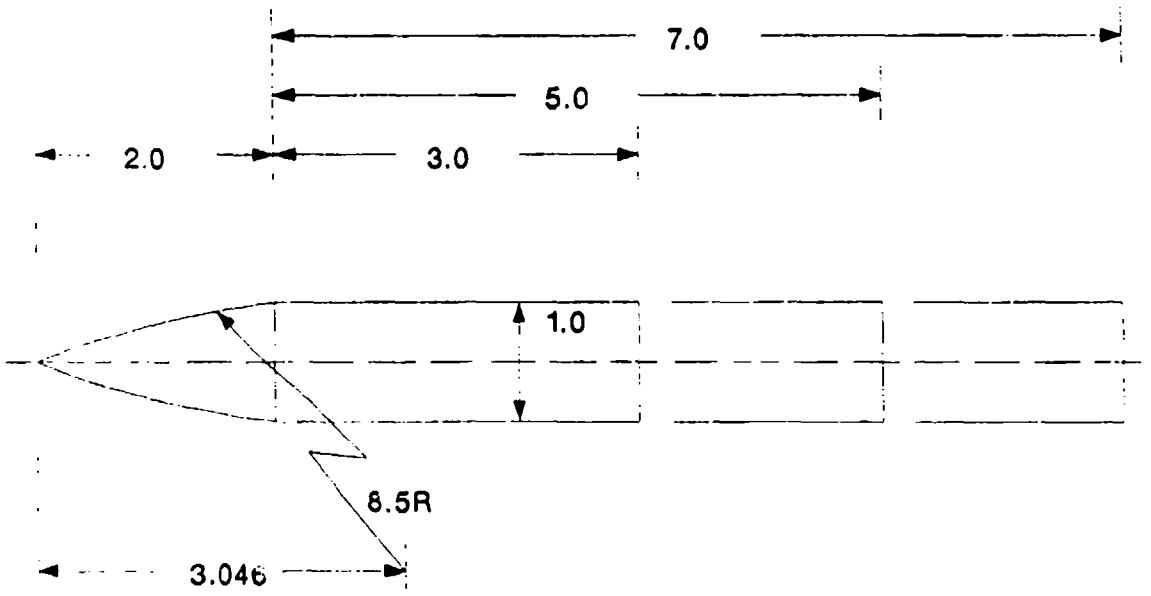

ALL DIMEN. ONS IN CALIBERS (ONE CALIBER = 20. mm)

Figure 2. Geometry of Army-Navy spinner rocket

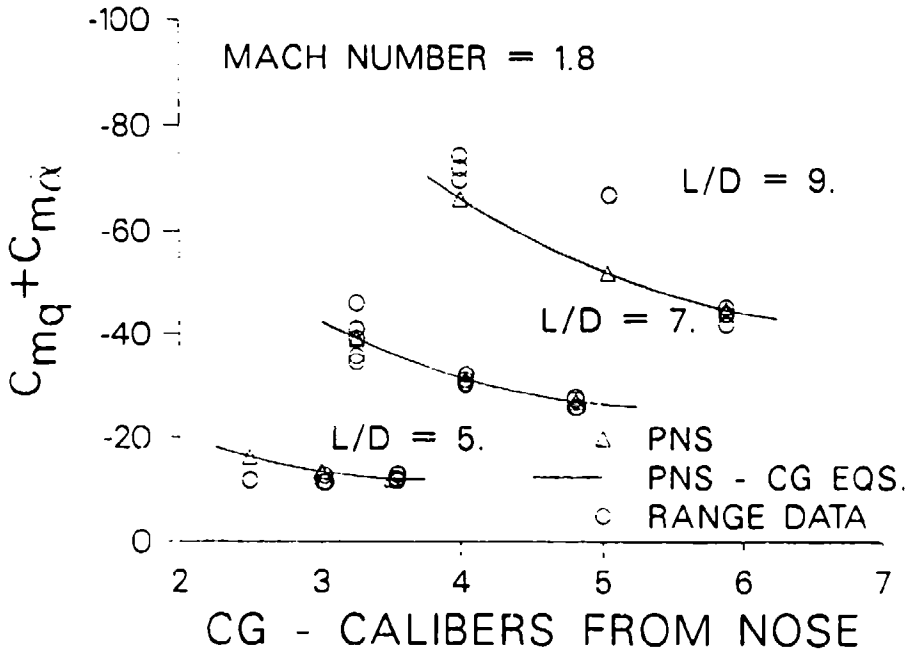

Figure 3. Pitch damping moment coefficient, Army-Navy spinner rocket, computation and experiment, Mach = 1.8

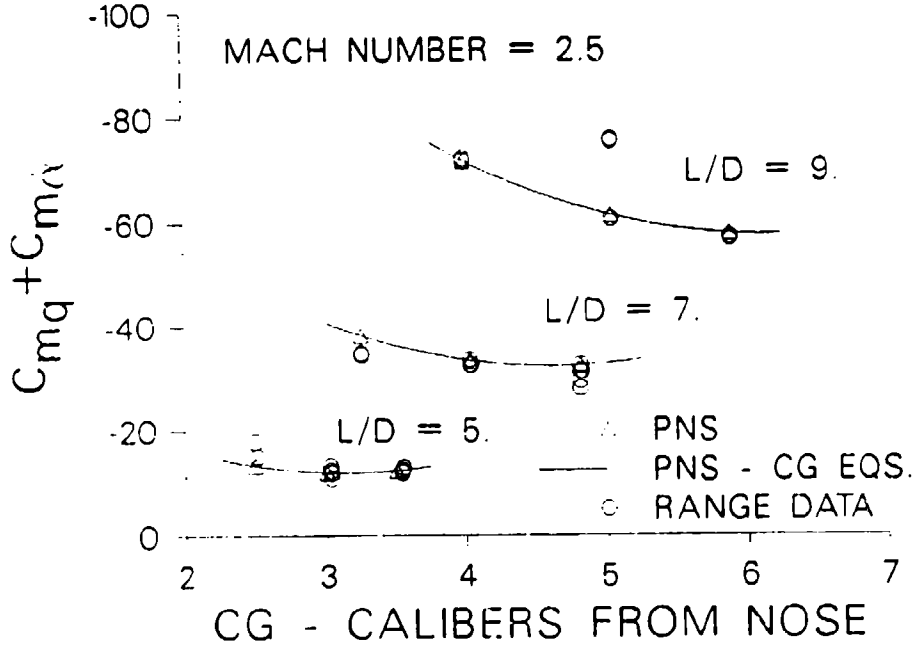

Figure 4. Pitch damping moment coefficient, Army-Navy spinner rocket, computation and experiment, Mach = 2.5

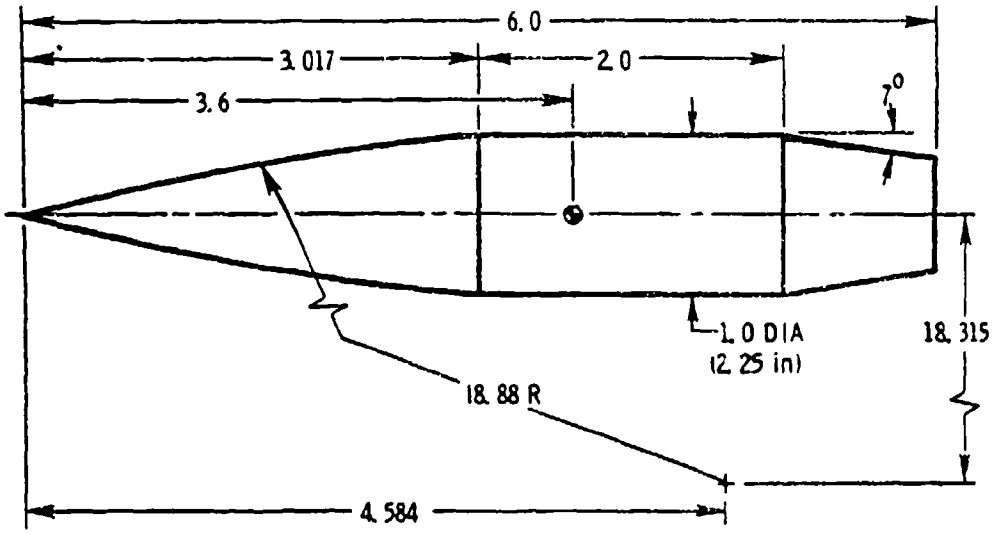

Figure 5. Experimental SOCBT configuration

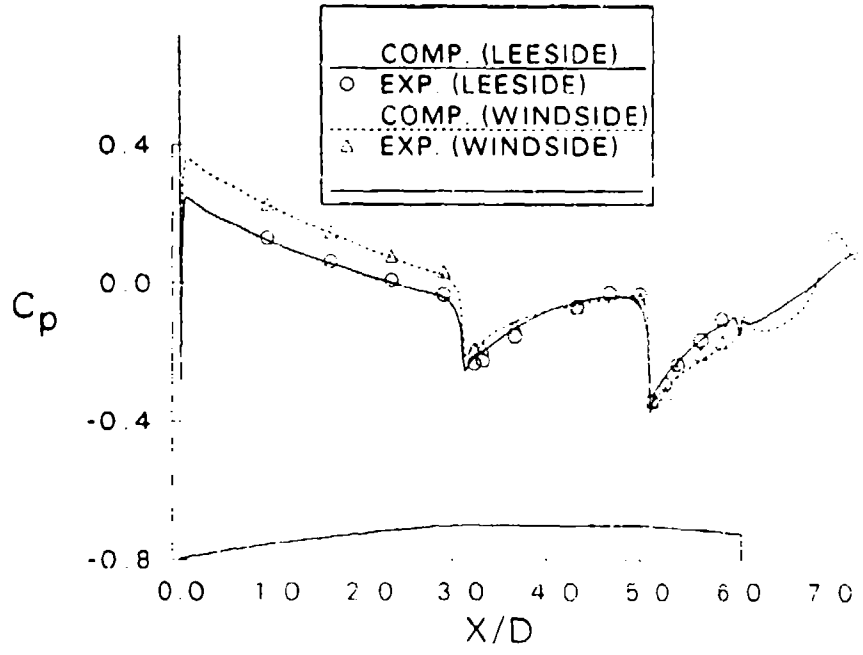

Figure 6. Longitudinal surface pressure distribution, SOCBT projectile, $M_\infty = 1.1$, $\alpha = 4°$

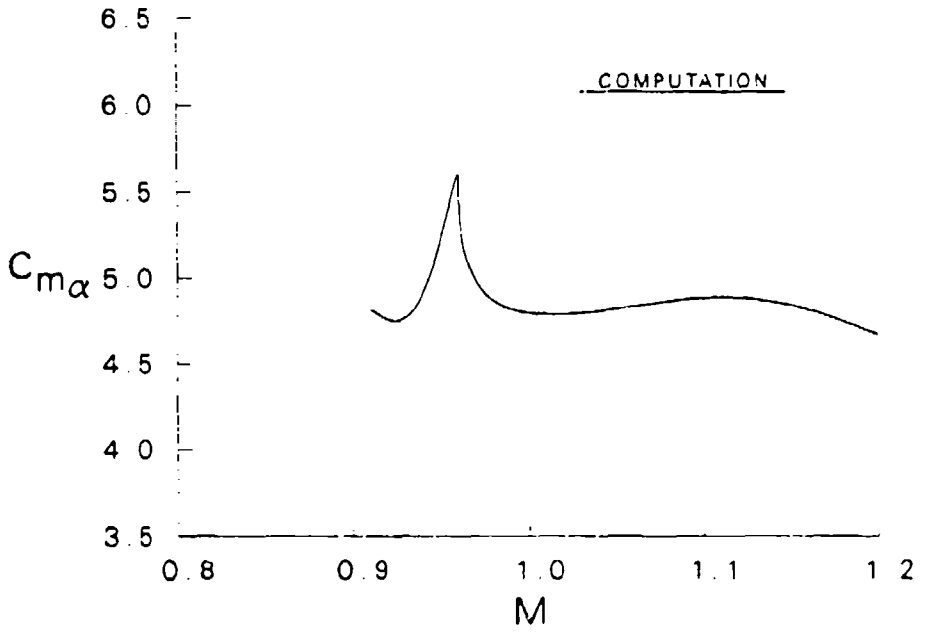

Figure 7. Slope of pitching moment coefficient vs Mach number, SOCBT

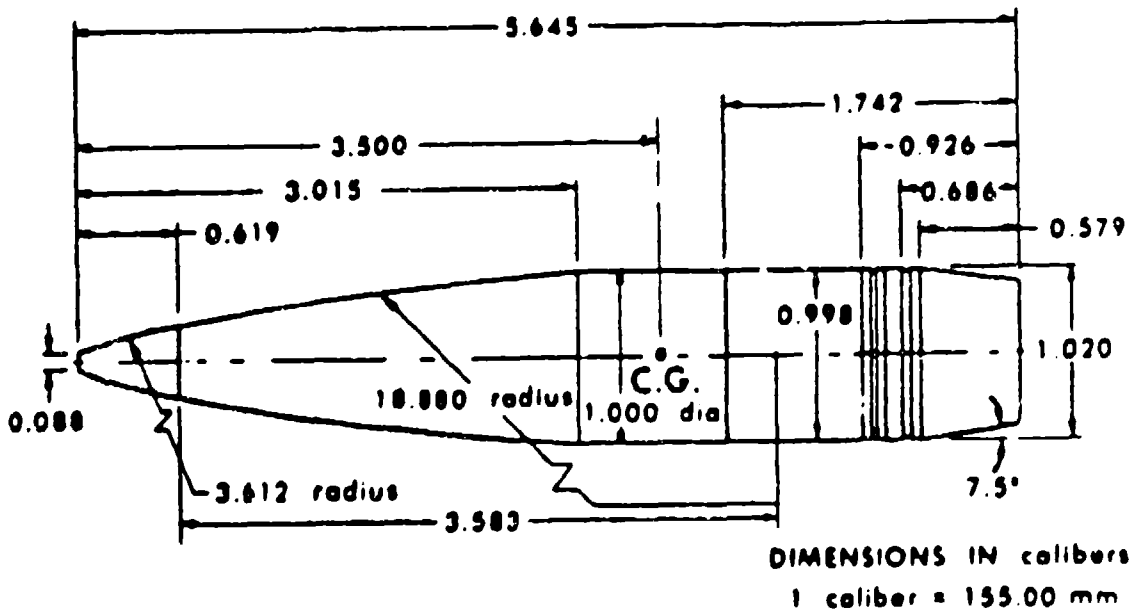

Figure 8. M549 projectile

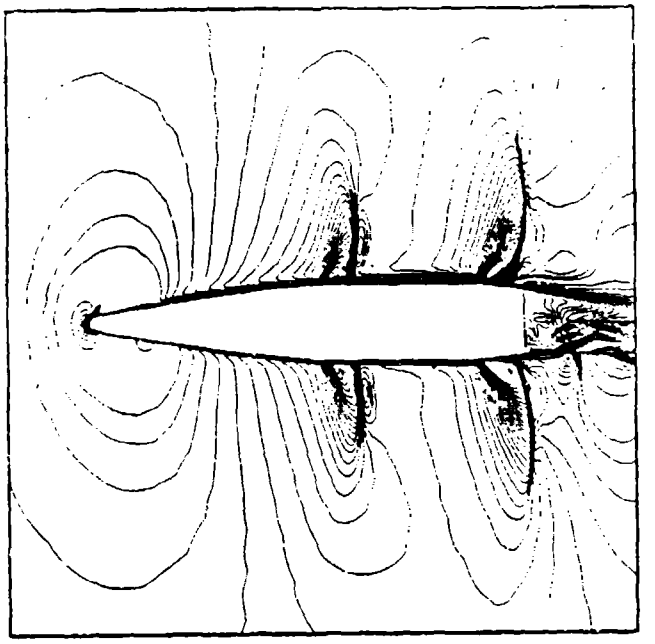

Figure 9. Mach contours of M549 projectile, $M_\infty = 0.94$, $\alpha = 2.0$

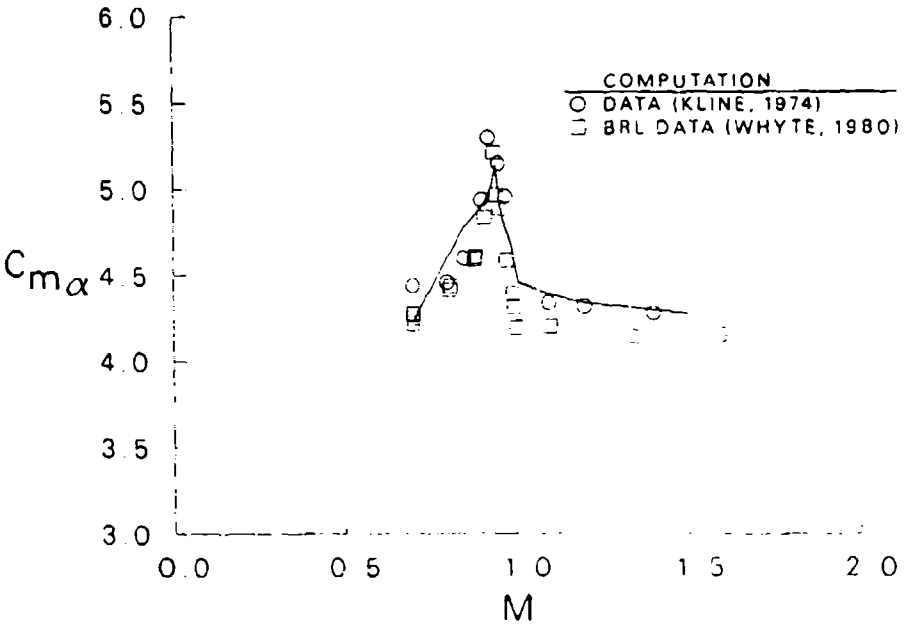

Figure 10. Slope of pitching moment coefficient vs Mach number, M549 projectile

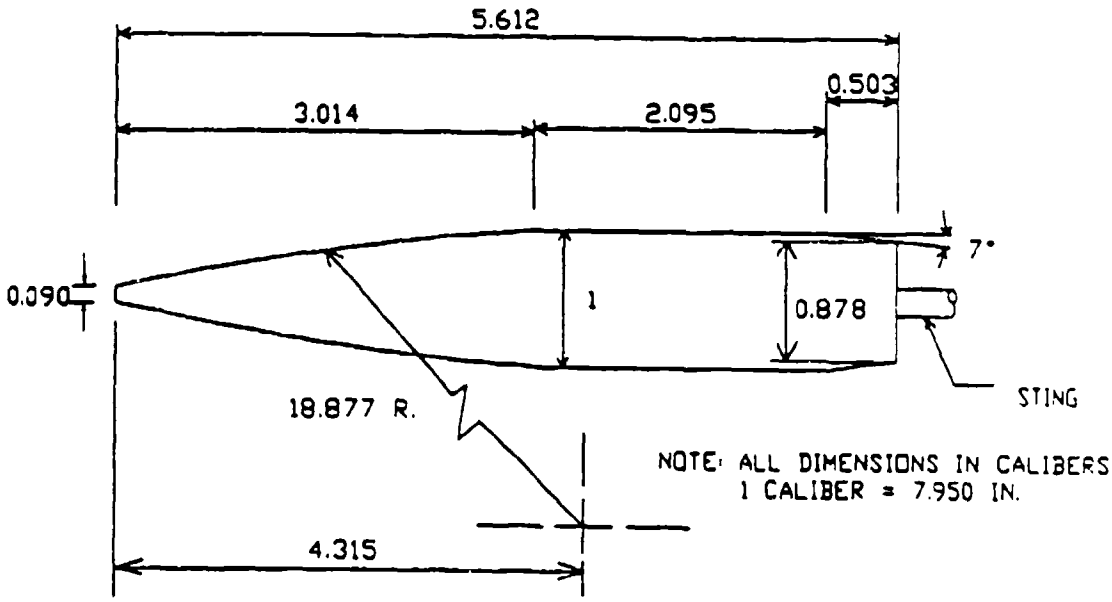

Figure 11. Experimental wind tunnel model with sting

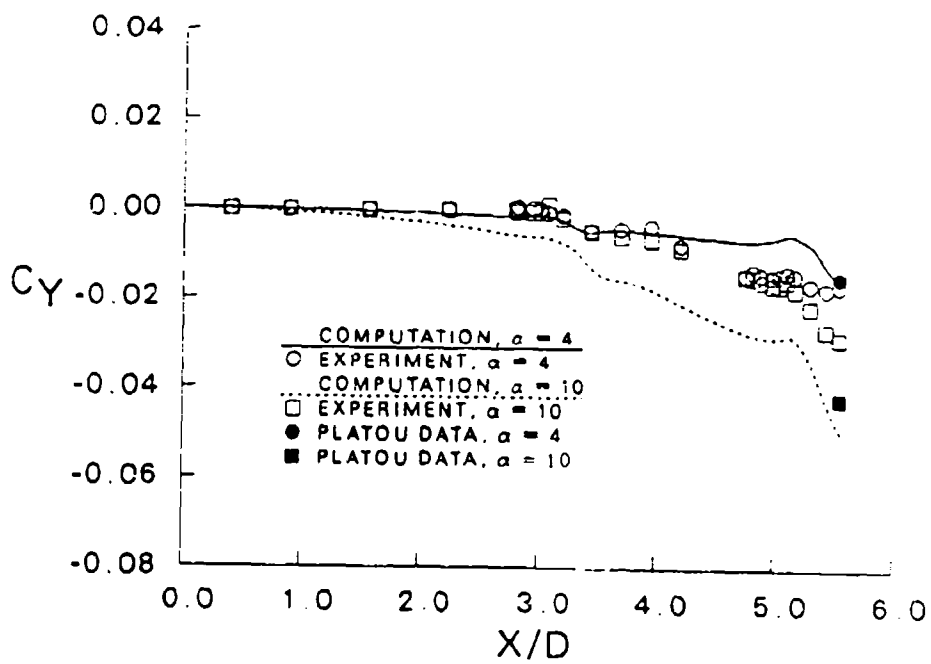

Figure 12. Development of Magnus force along the projectile, $M_\infty \approx 0.94$

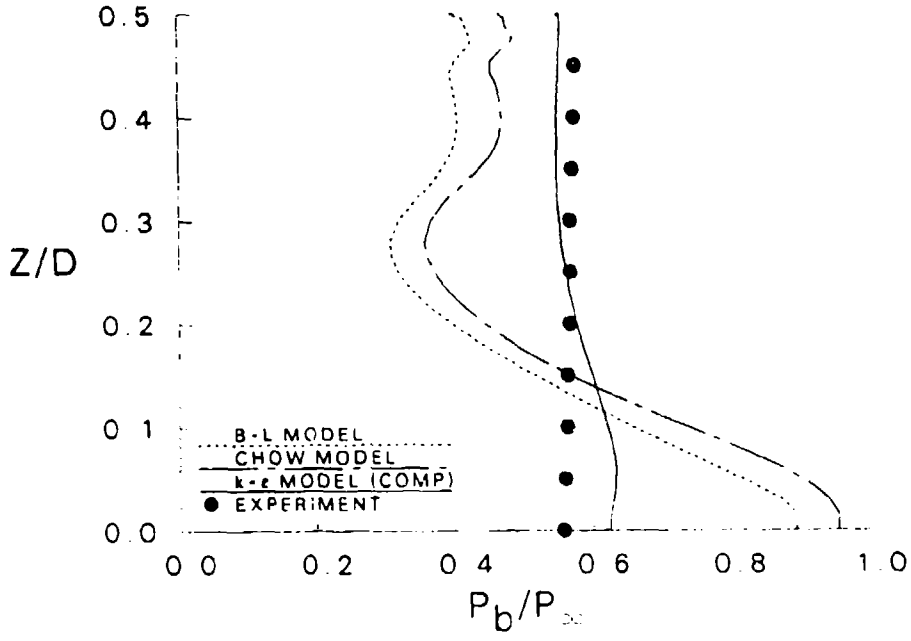

Figure 13. Base pressure distribution, computations and experiment

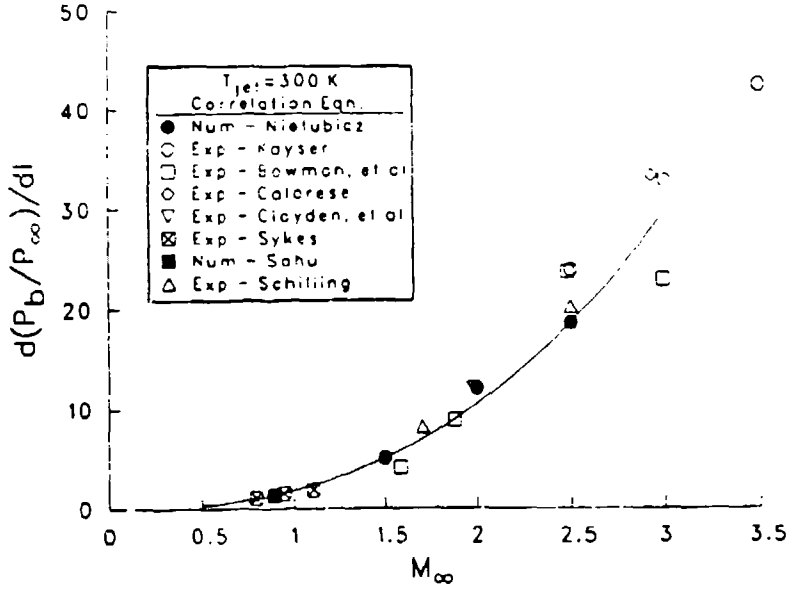

Figure 14. $d(P_b / P_\infty) / dl$ vs M_∞, computation and experiment, T_{oinj} = 300 K

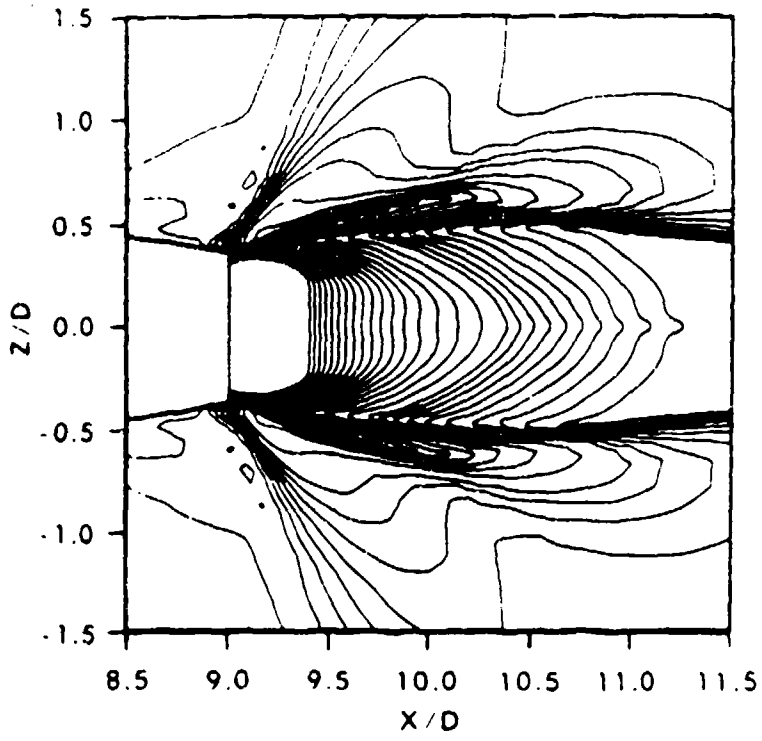

Figure 15. Computed density contours; experimental Schlieren photograph, $M_\infty = 2.0$, $M_j = 2.5$, $P_j / P_\infty = 9.0$, jet on

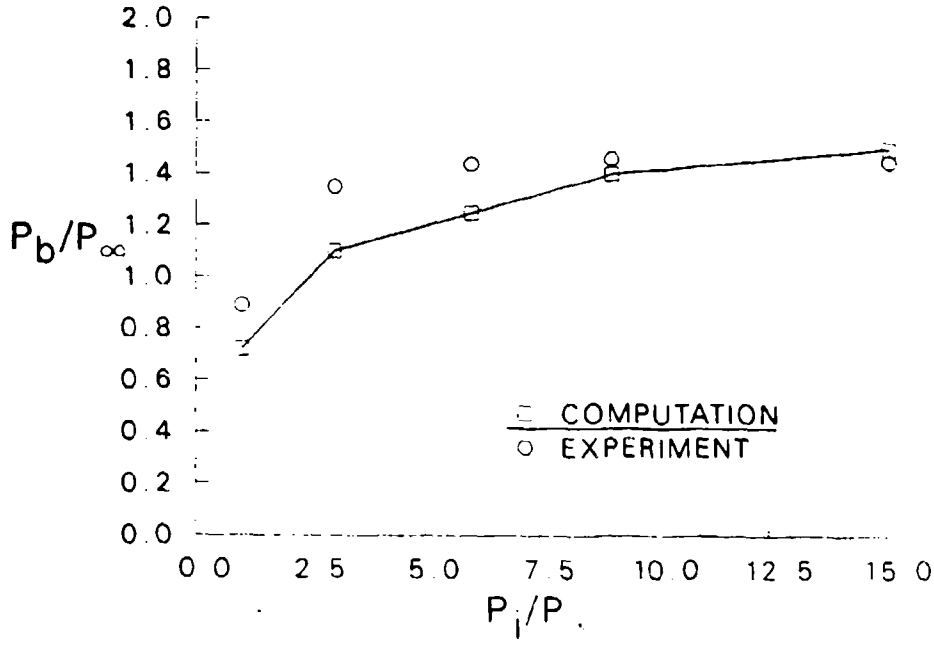

Figure 16. Variation of base pressure with jet pressure, M_∞ = 2.0, jet on

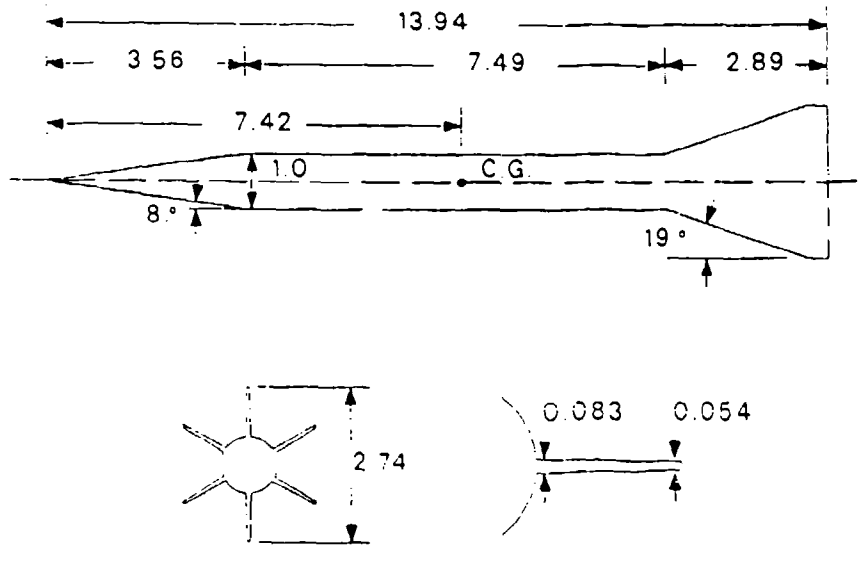

ALL DIMENSIONS IN CALIBERS (ONE CALIBER = 35.2 mm)

Figure 17. Geometry of M735 projectile

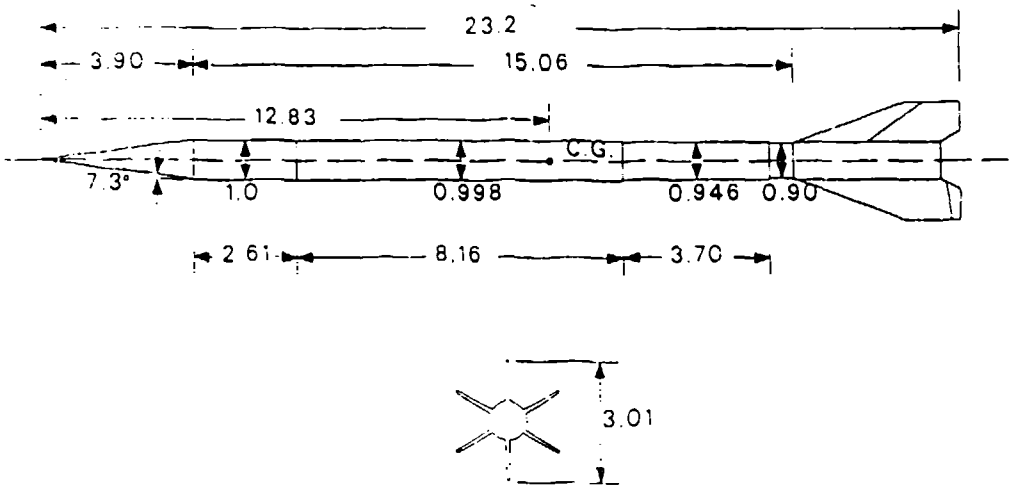

ALL DIMENSIONS IN CALIBERS (ONE CALIBER = 27.05 mm)

Figure 18. Geometry of M829 projectile

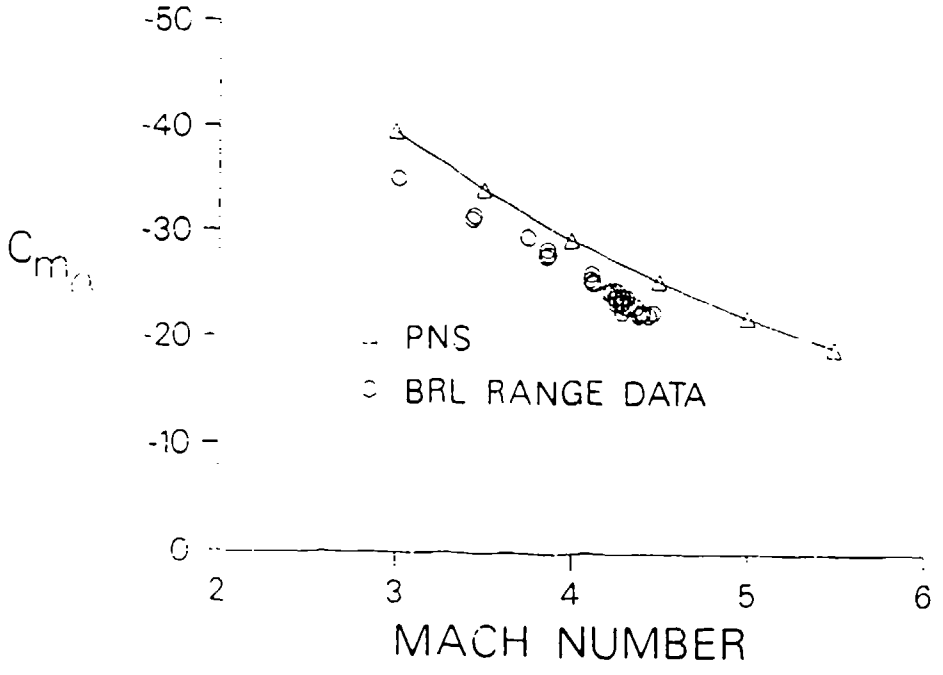

Figure 19. Pitching moment coefficient, M735, computation and experiment

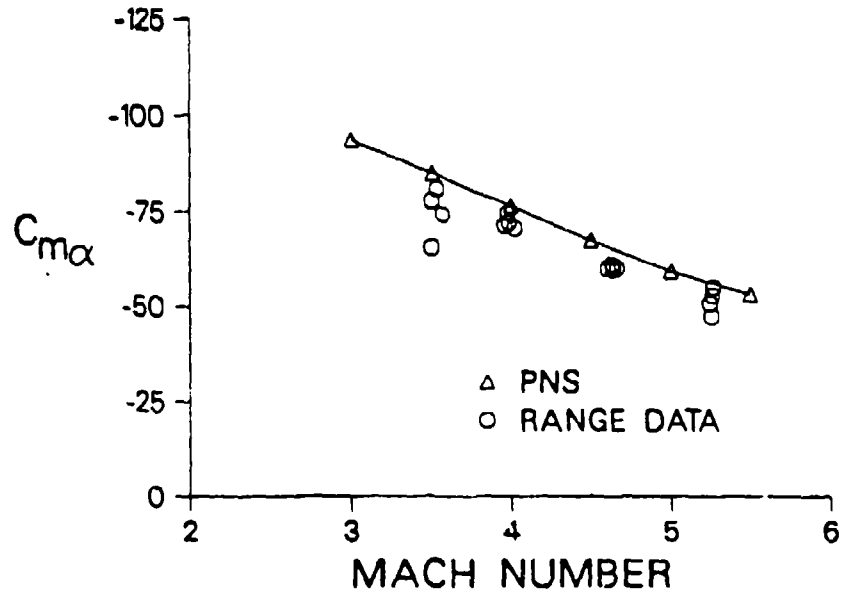

Figure 20. Pitching moment coefficient, M829, computation and experiment

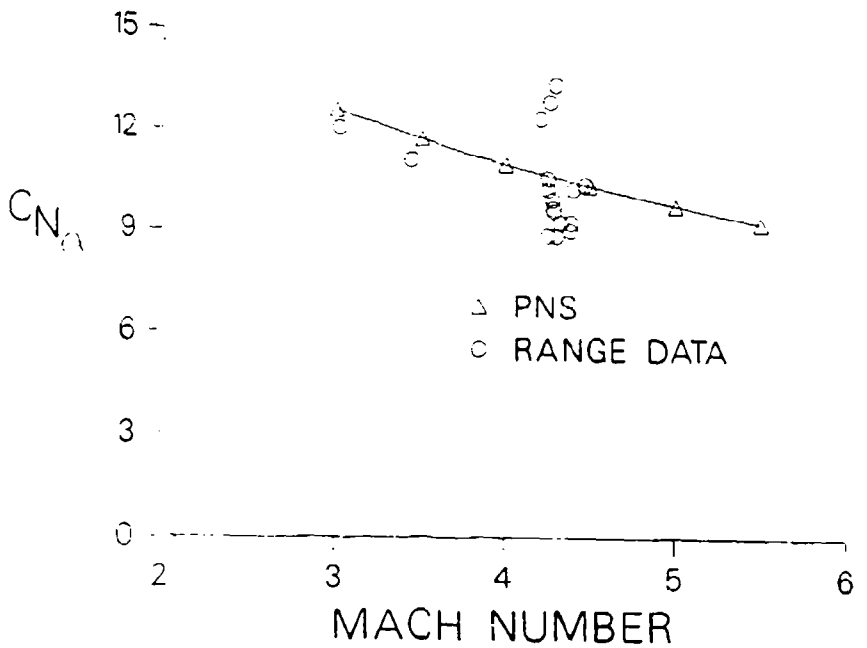

Figure 21. Normal force coefficient, M735, computation and experiment

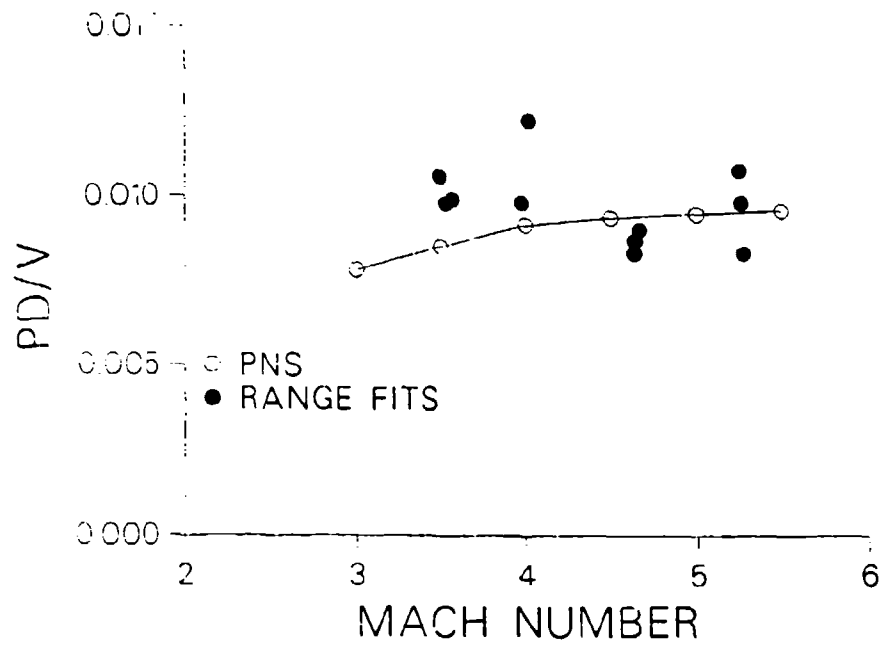

Figure 22. Equilibrium spin rate, M829, computation and experiment

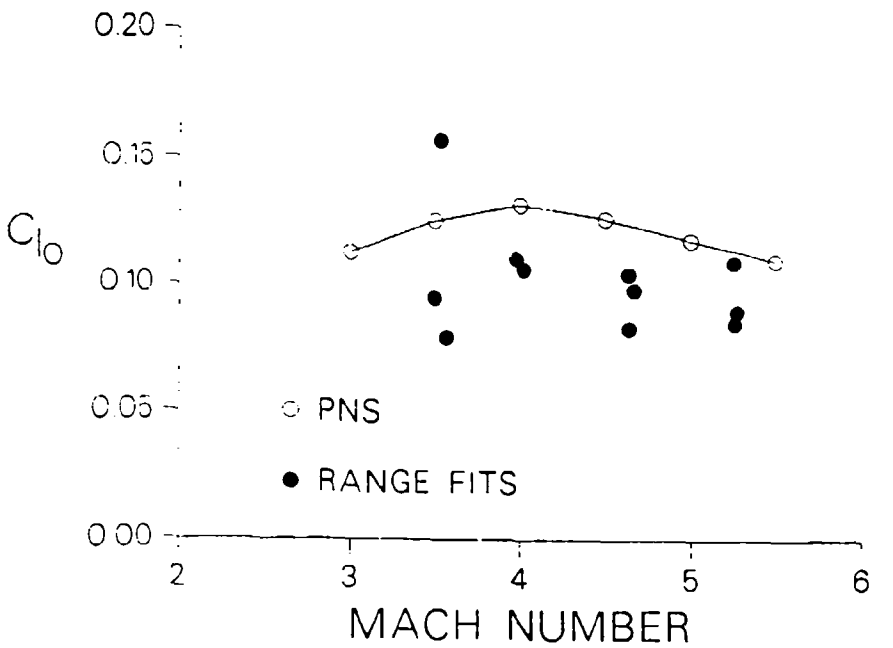

Figure 23. Roll producing moment coefficient, M829, computation and experiment

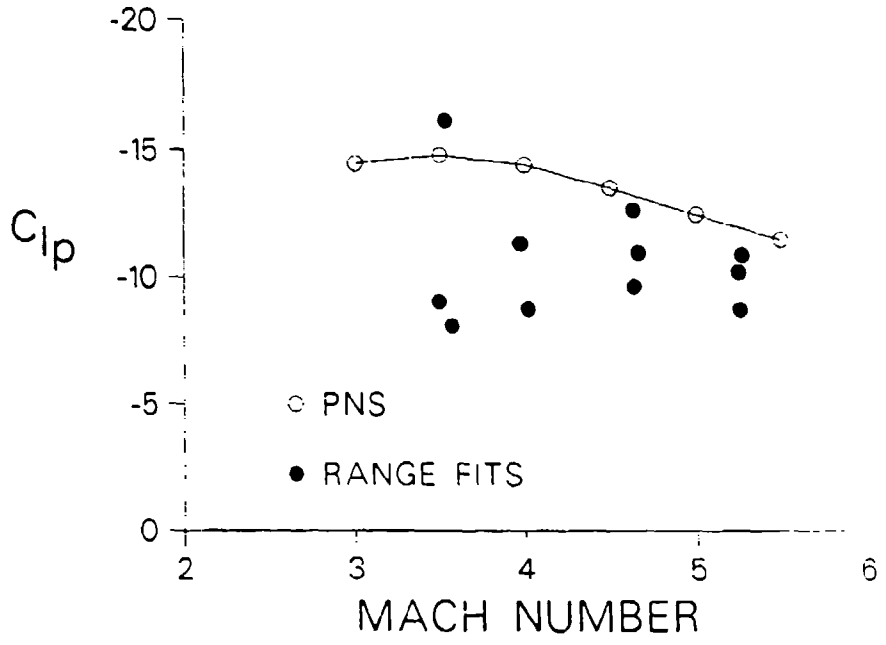

Figure 24. Roll damping coefficient, M829, computation and experiment

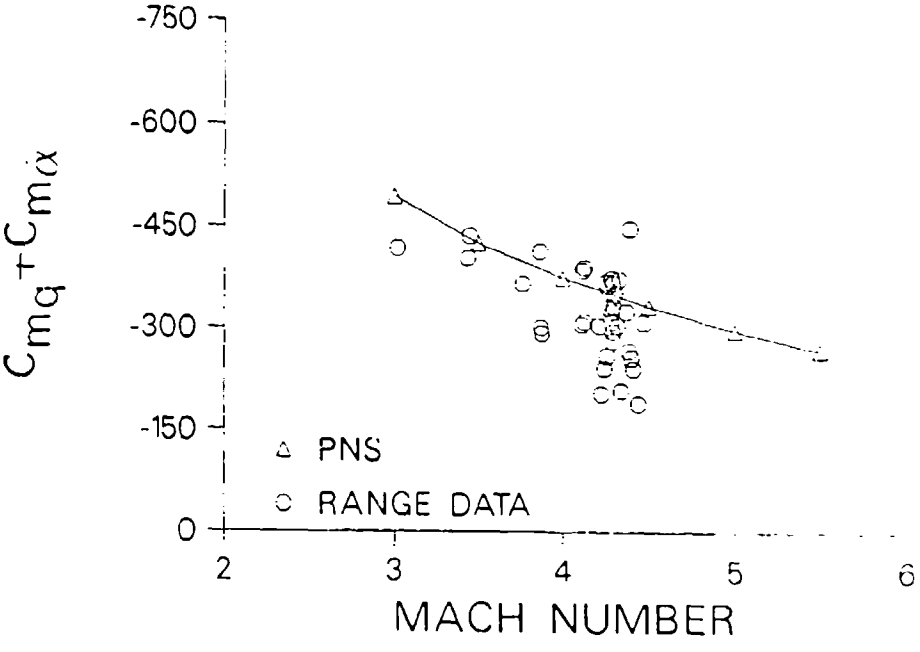

Figure 25. Pitch damping moment coefficient, M735, computation and experiment

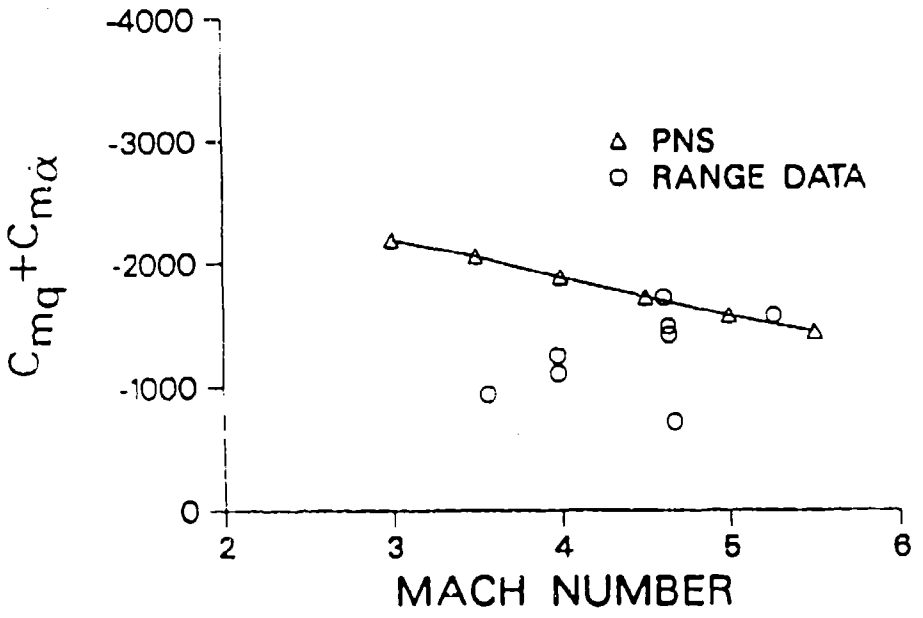

Figure 26. Pitch damping moment coefficient, M829, computation and experiment

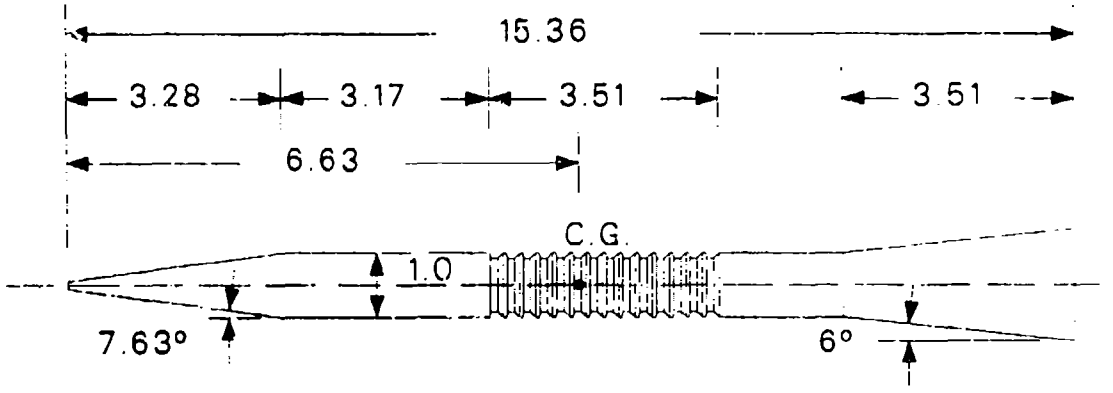

ALL DIMENSIONS IN CALIBERS (ONE CALIBER = 8.28 mm)

Figure 27. Baseline flare stabilized projectile geometry

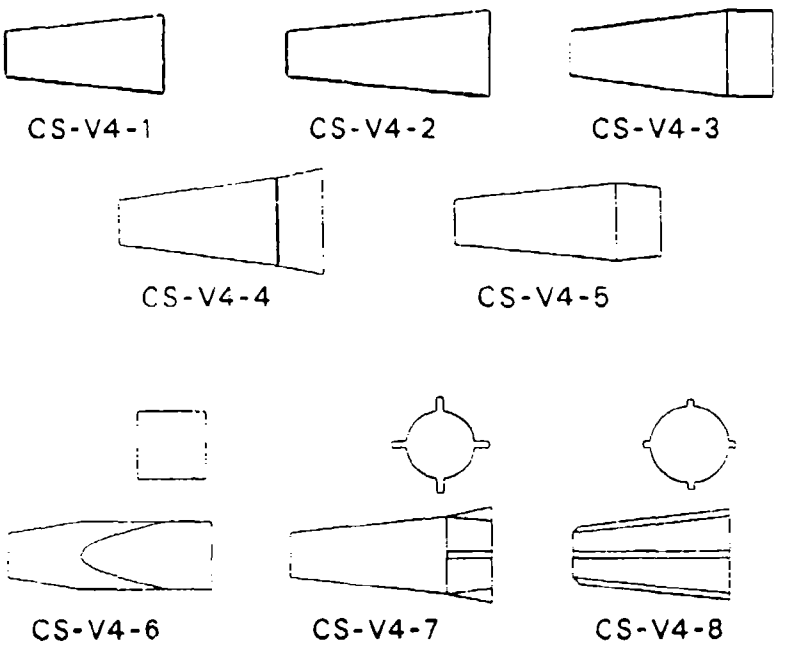

Figure 28. Parametric flare afterbody geometries

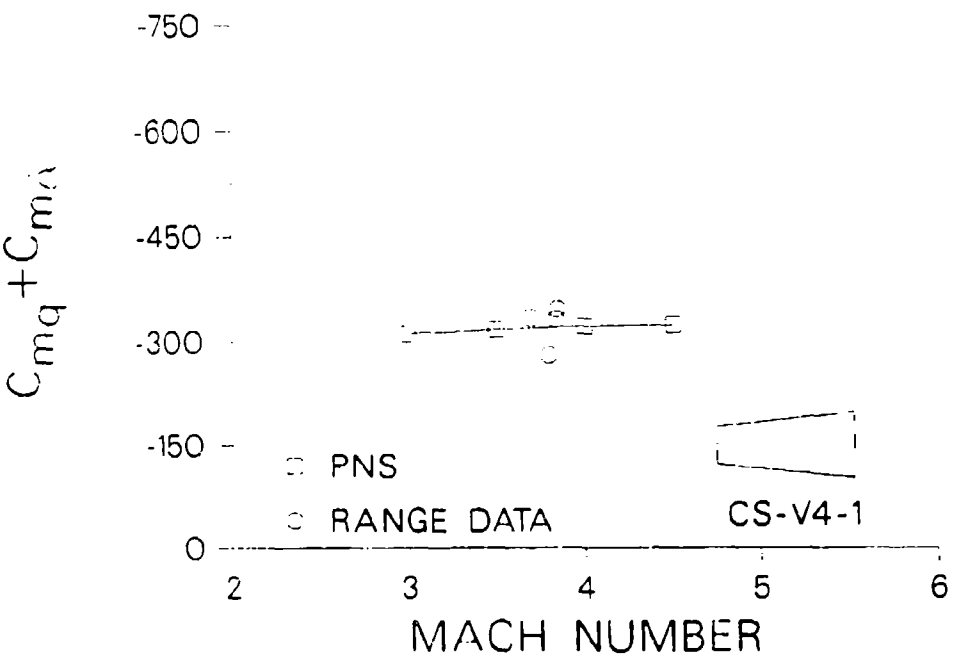

Figure 29. Pitch damping moment coefficient, flare V4-1, computation and experiment

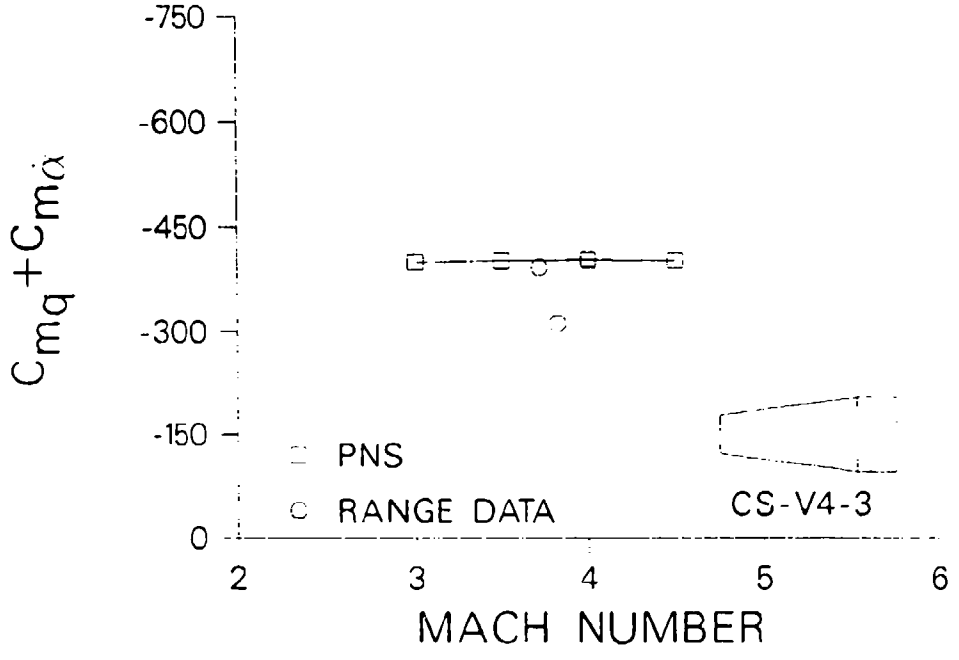

Figure 30. Pitch damping moment coefficient, flare V4-3, computation and experiment

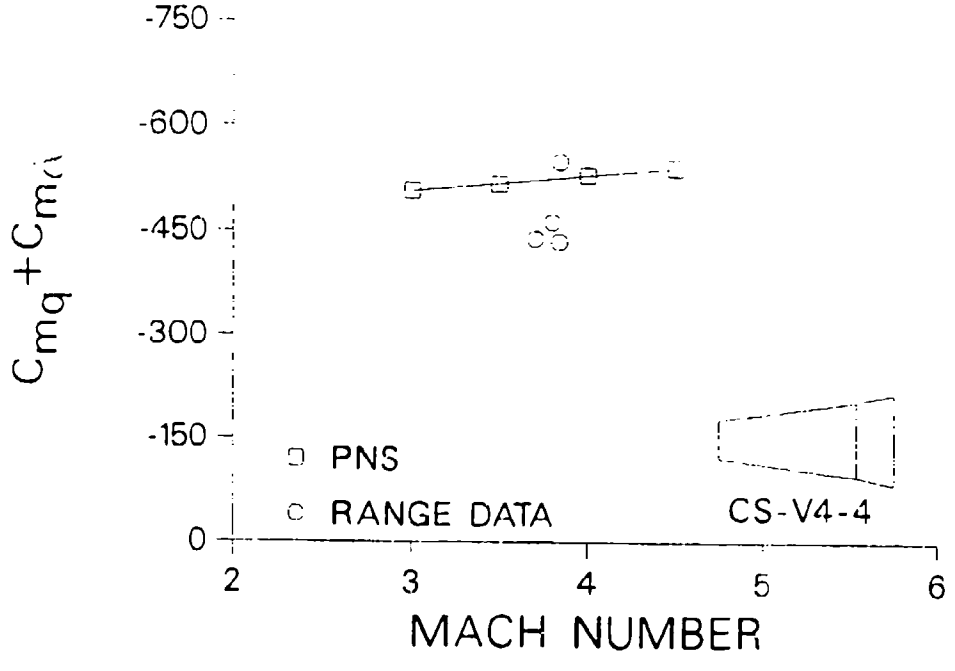

Figure 31. Pitch damping moment coefficient, flare V4-4, computation and experiment

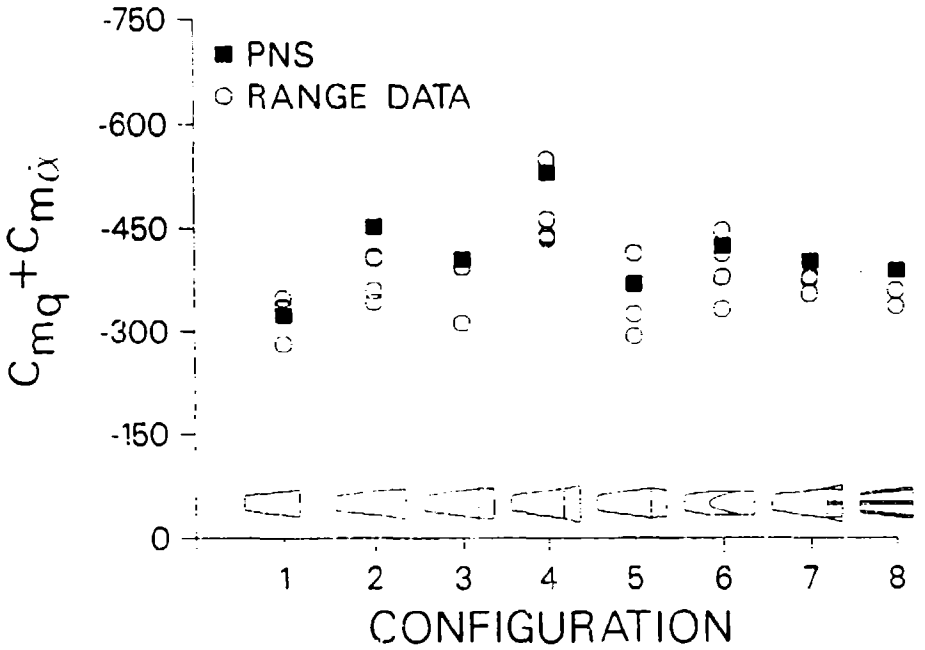

Figure 32. Pitch damping moment coefficient, flares at Mach 4, computation and experiment

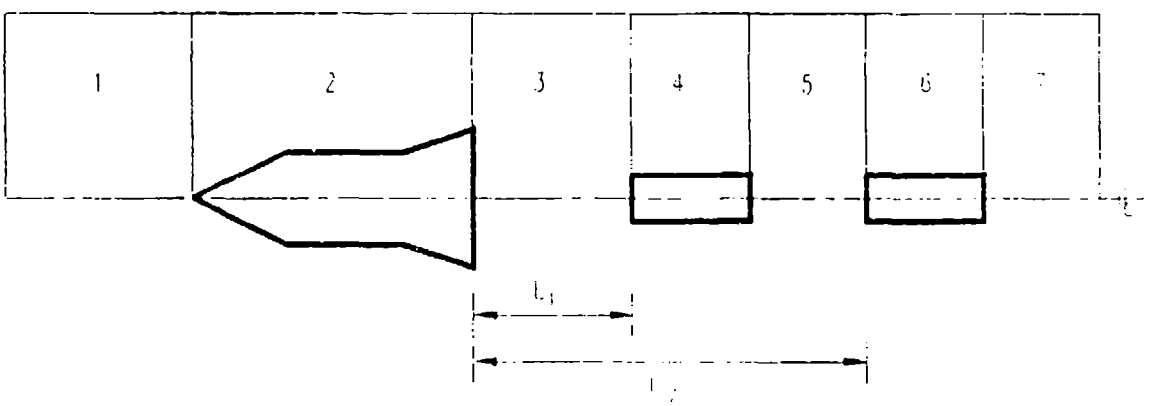

Figure 33. Schematic diagram of multi-body problem

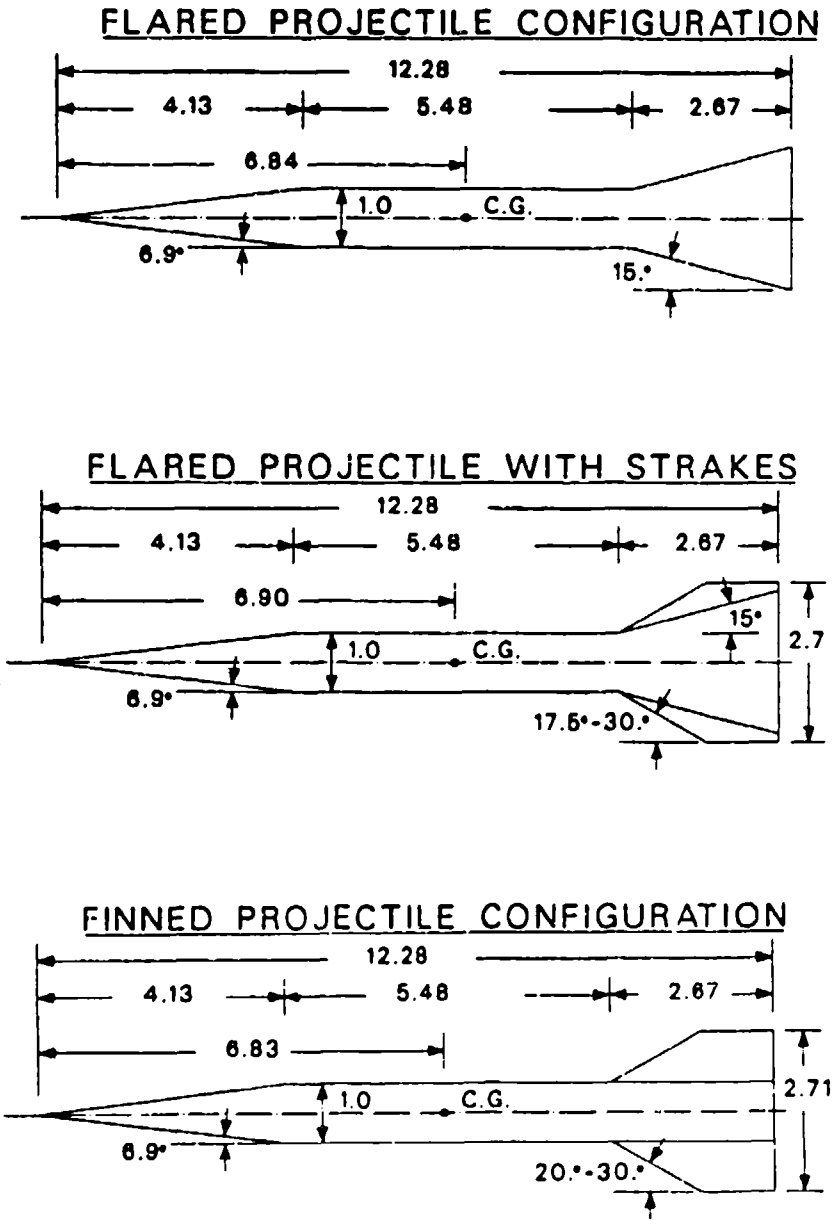

Figure 34. Scorpion projectile configurations

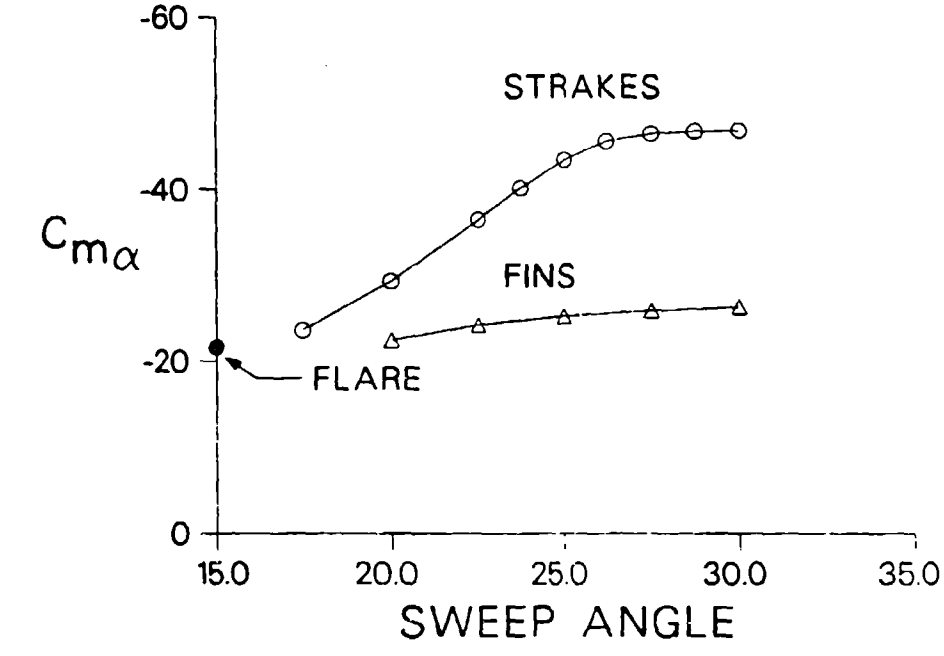

Figure 35. Pitching moment coefficient, Scorpion configurations, computation vs sweep angle of fins and strakes

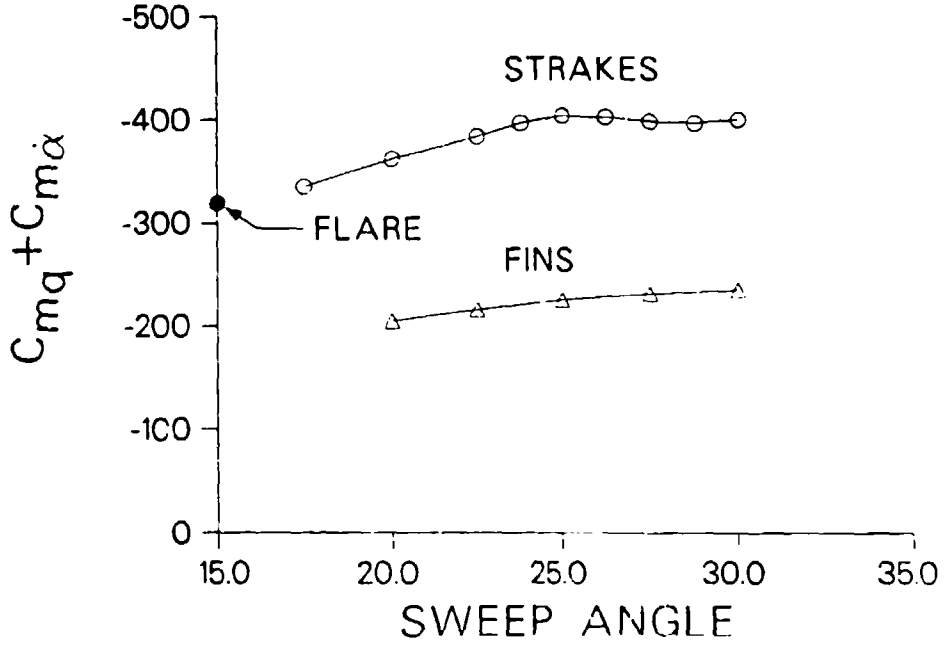

Figure 36. Pitch damping moment coefficient, Scorpion configurations, computation vs sweep angle of fins and strakes

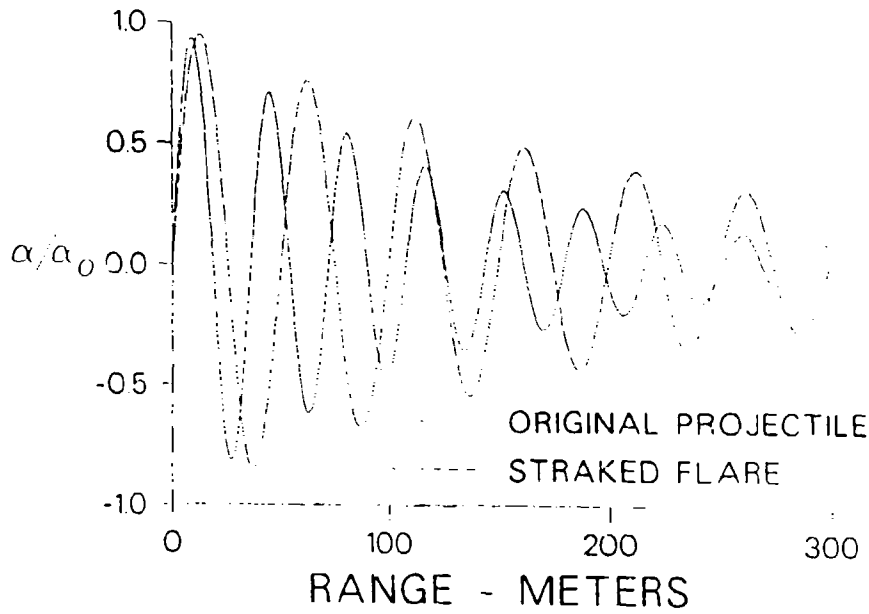

Figure 37. Prediction of pitch damping motion, Scorpion original and optimized configurations

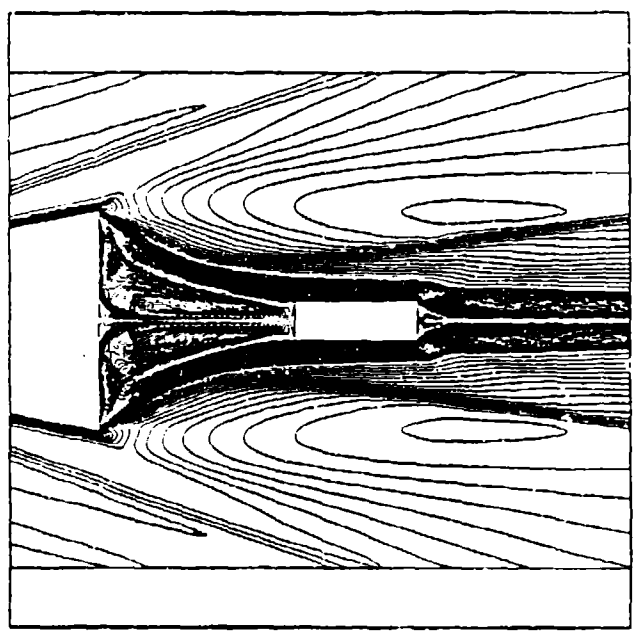

Figure 38. Mach contours in the base region with segment at 2 calibers from base, $M_\infty = 4.4$, $\alpha = 0.0$

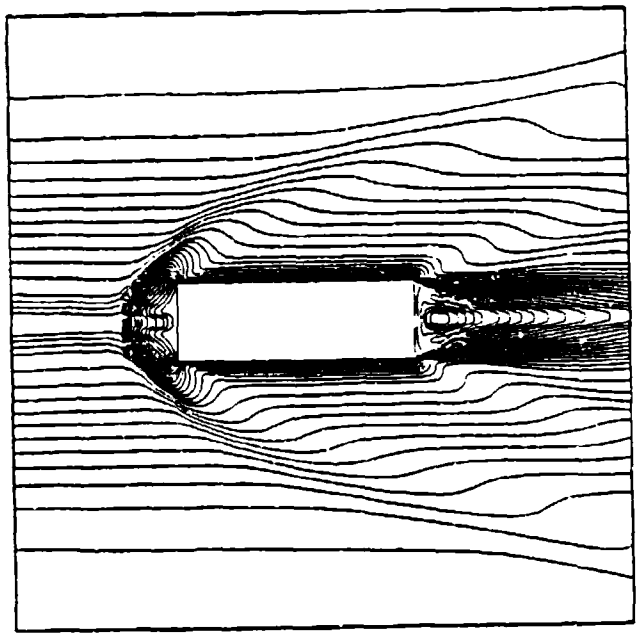

Figure 39. Mach contours in the base region with segment at 10 calibers from base, $M_\infty = 4.4$, $\alpha = 0.0$

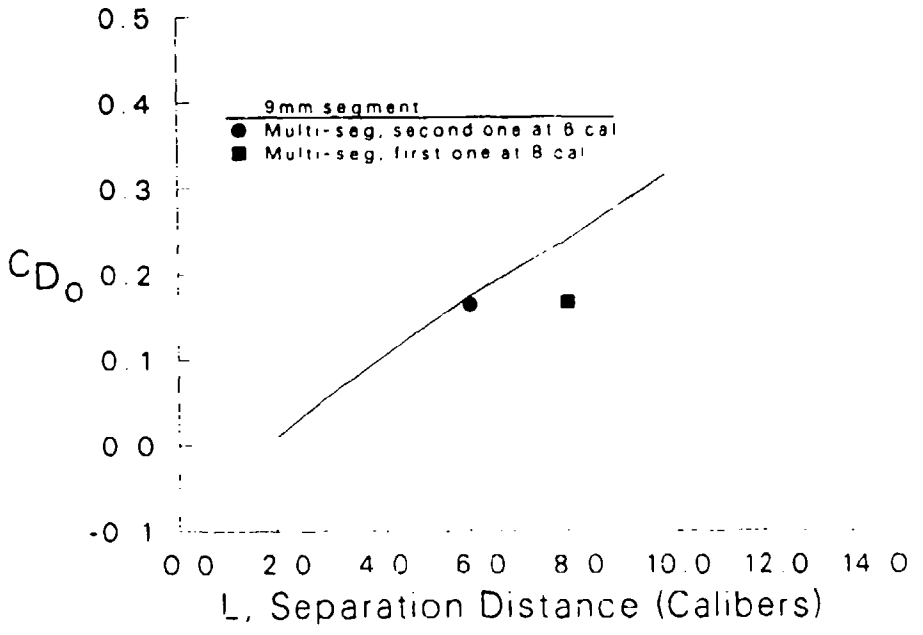

Figure 40. Segment aerodynamic drag coefficient vs separation distance from the base, $M_\infty = 4.4$, $\alpha = 0.0$

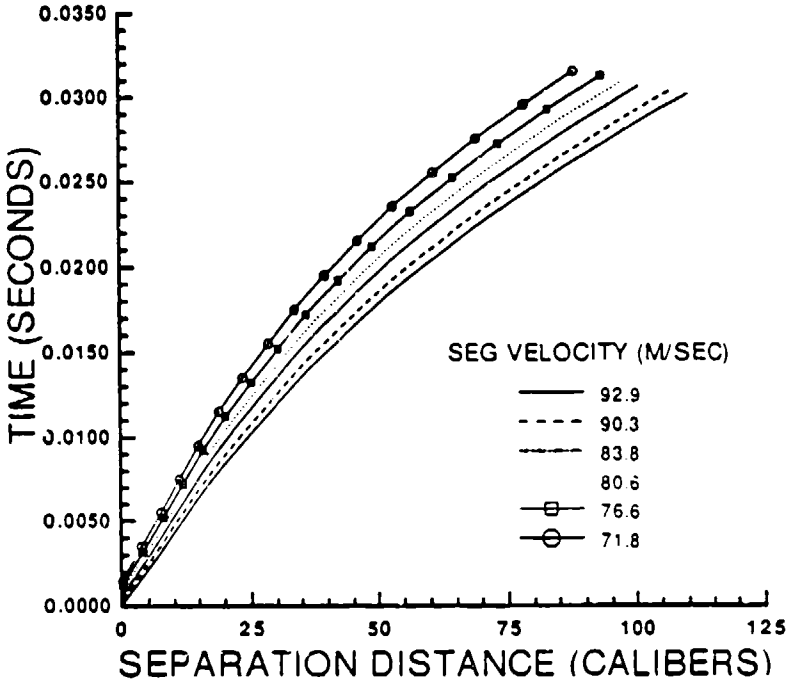

Figure 41. Trajectory predictions of segment separation distance from parent projectile, 9mm segment

CONTROL PROJECTILE CONFIGURATION

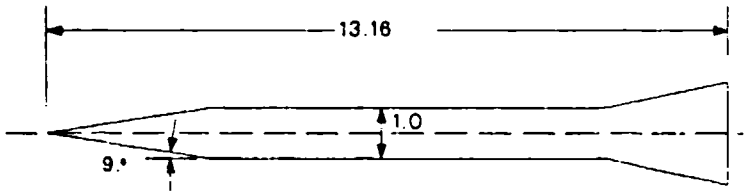

EXTENDED PROJECTILE CONFIGURATION

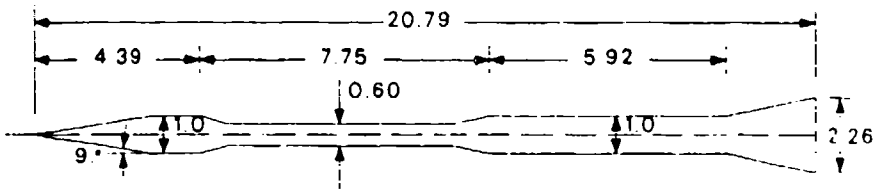

ALL DIMENSIONS IN CALIBERS (ONE CALIBER = 7 62 mm)

Figure 42. Launch and extended configurations for extended rod concept

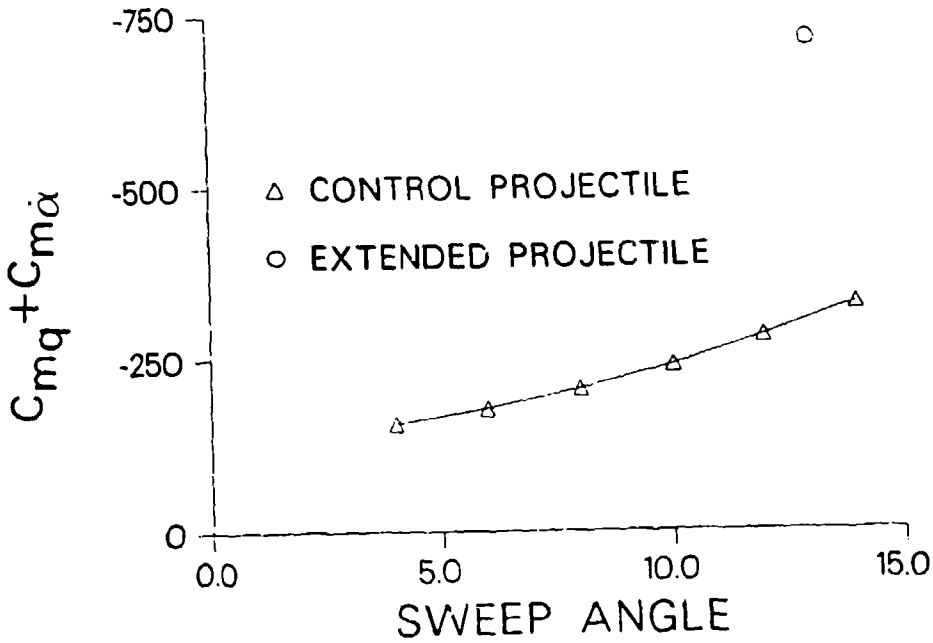

Figure 43. Pitch damping moment coefficient, extended rod configurations, computation vs flare sweep angle

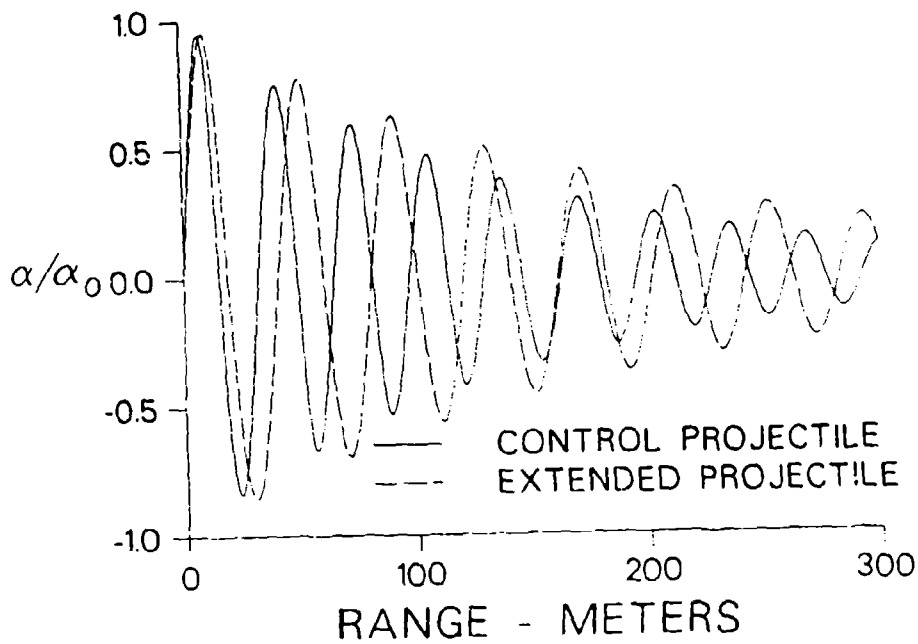

Figure 44. Pitch damping motion, extend rod configurations, prediction

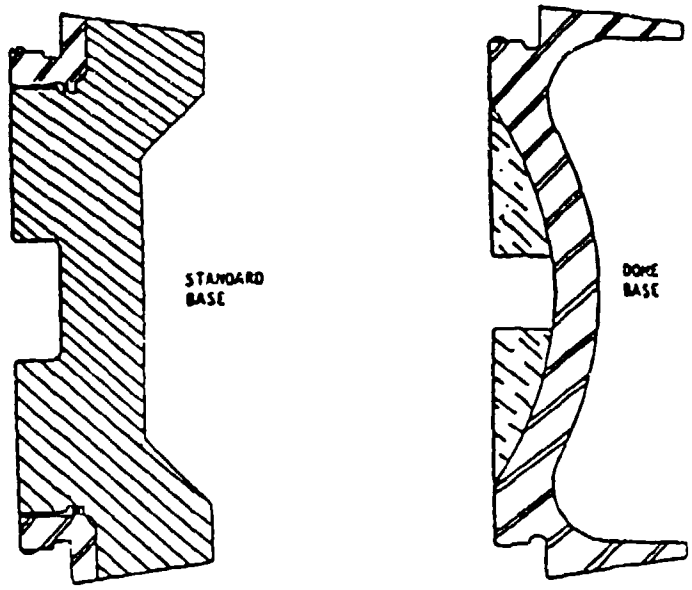

Figure 45. Base cavity configurations

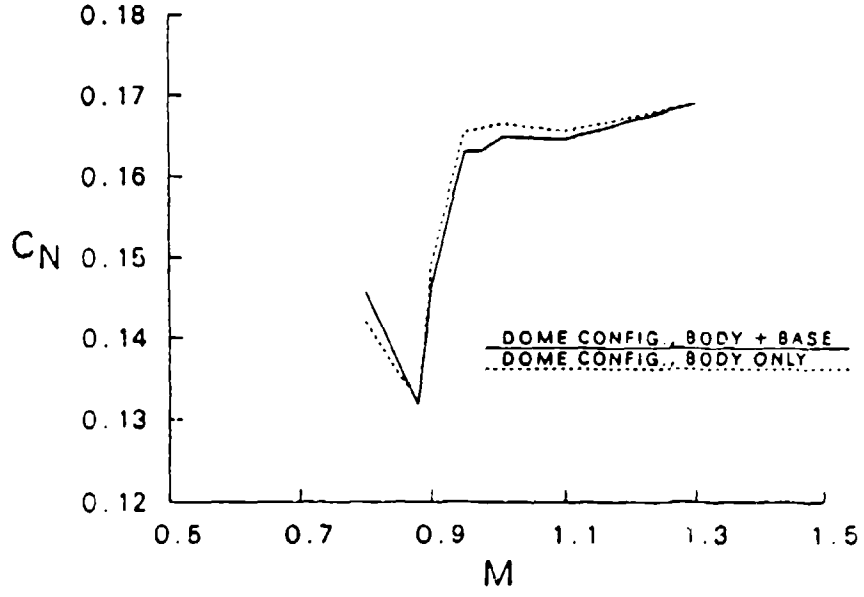

Figure 46. Normal force coefficient vs Mach number for standard and dome base

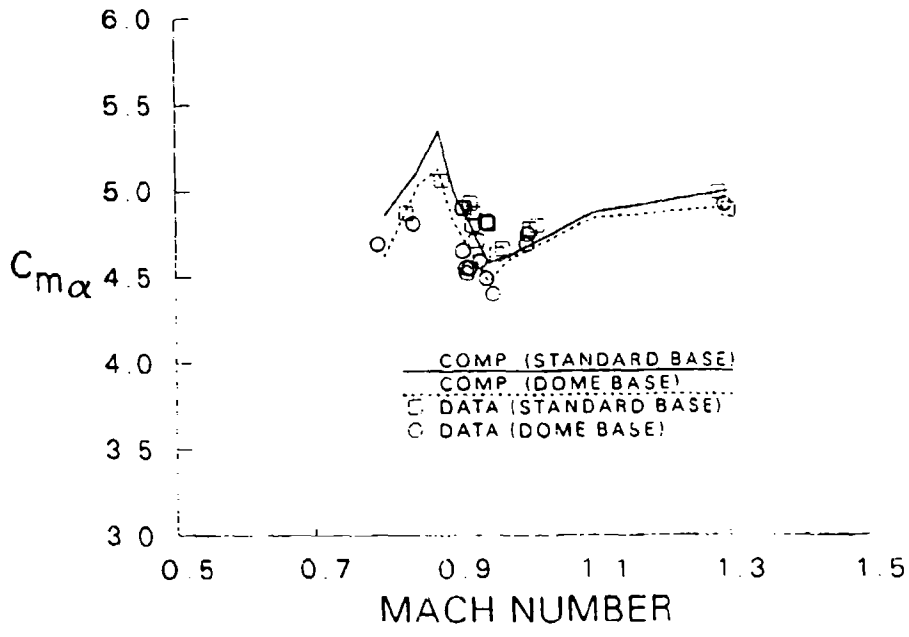

Figure 47. Slope of pitching moment coefficient vs Mach number for standard and dome base

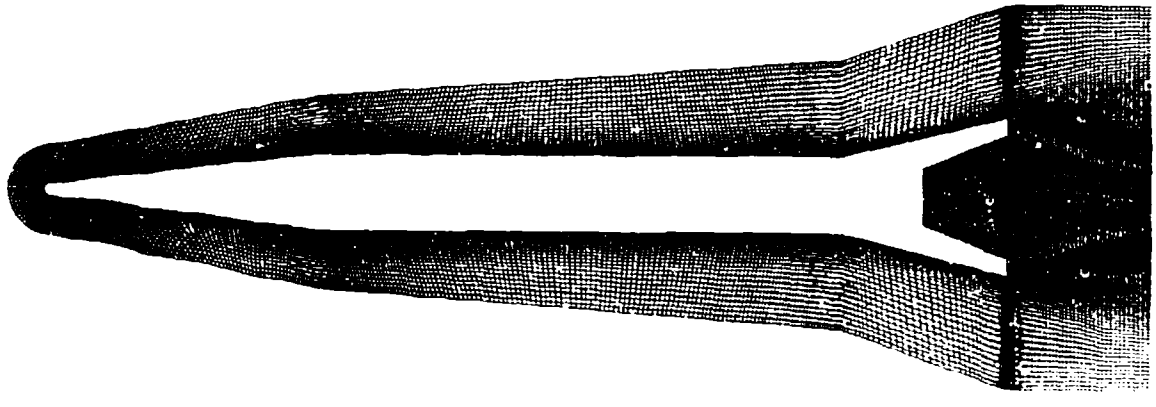

Figure 48. Computational model of M865

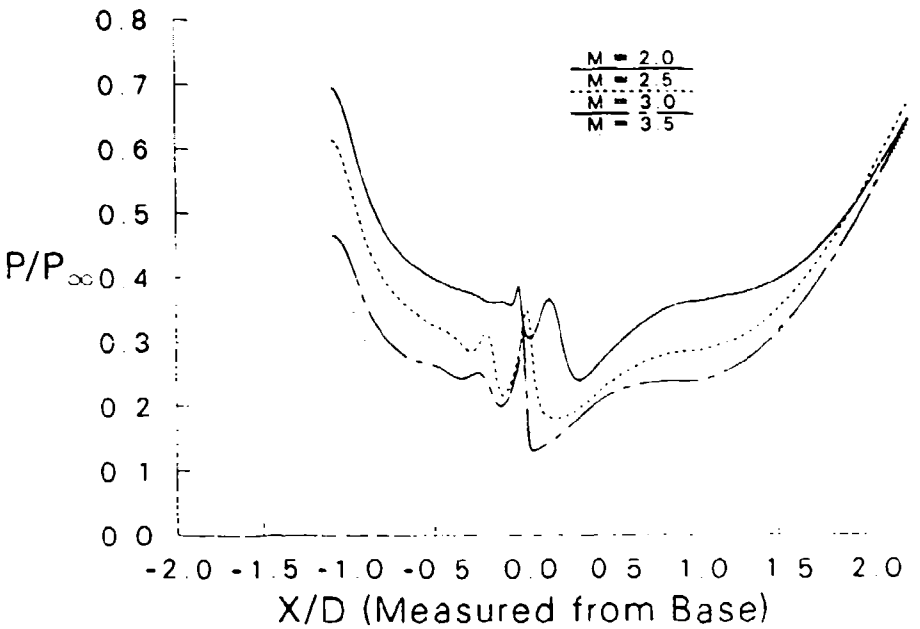

Figure 49. Wake centerline pressure distributions, α = 0.0°, (orginal configuration)

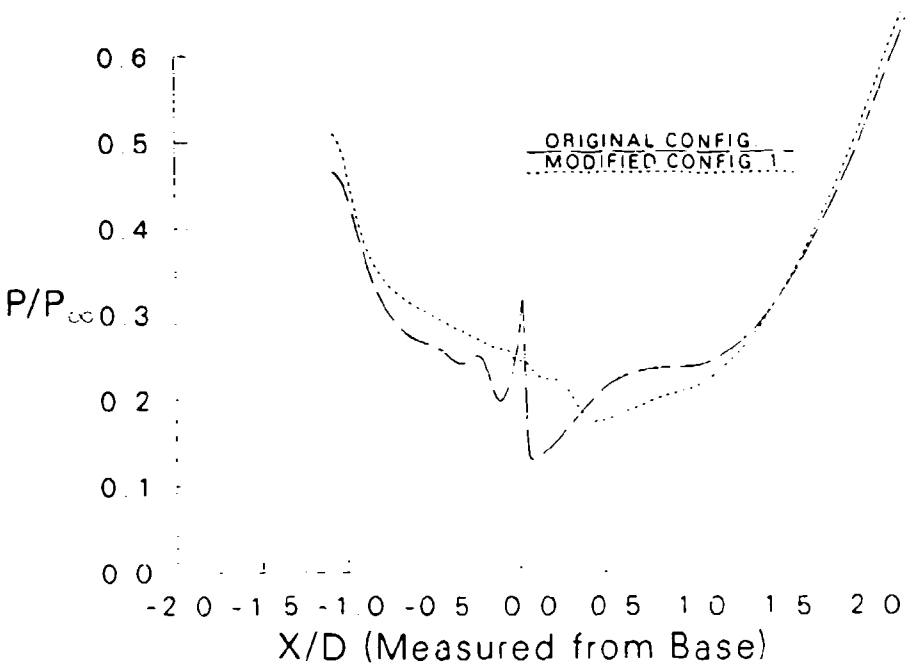

Figure 50. Wake centerline pressure distribution, M_∞ = 3.0, α = 0.0°, (modified configuration)

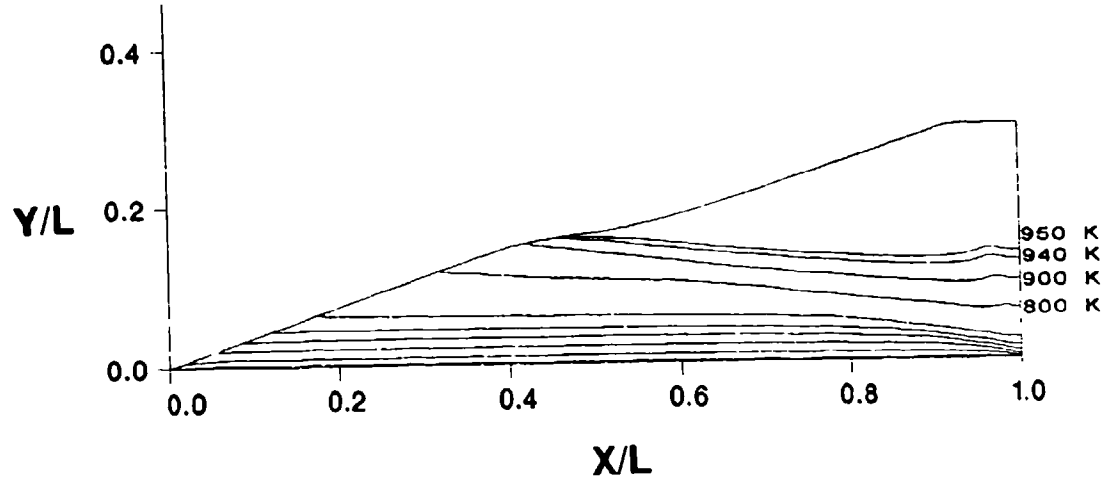

Figure 51. Temperature contours, M829, aluminum oxide coating, flight time = 2.0 seconds

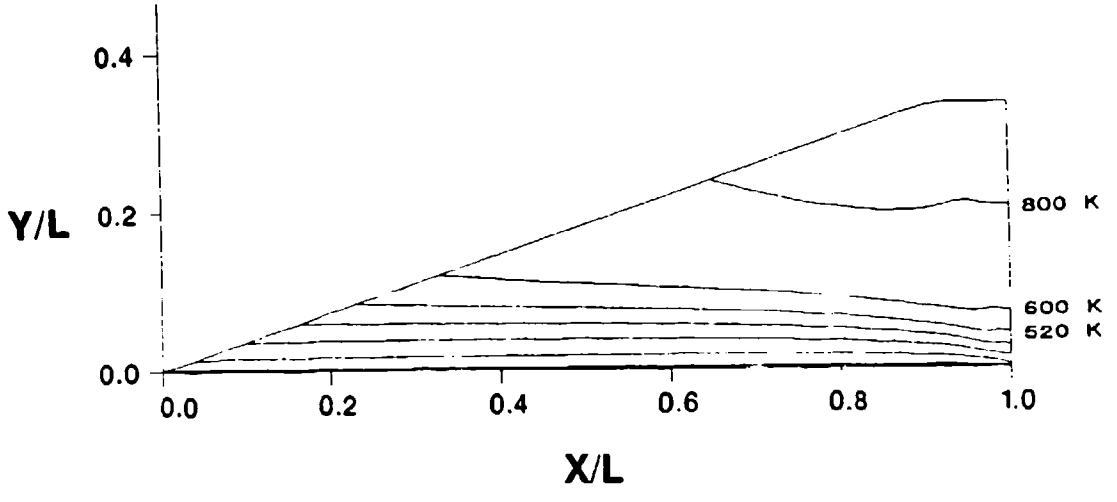

Figure 52. Temperature contours, M829, fiber/epoxy coating, flight time = 2.0 seconds

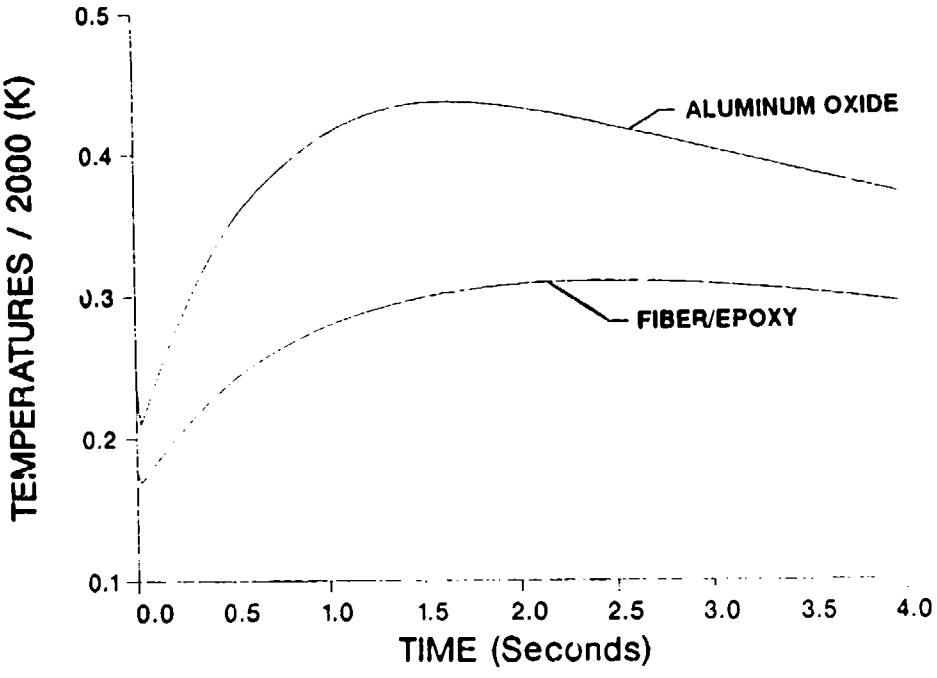

Figure 53. Temperature at M829 fin leading edge vs flight time, aluminum oxide and fiber/epoxy coatings

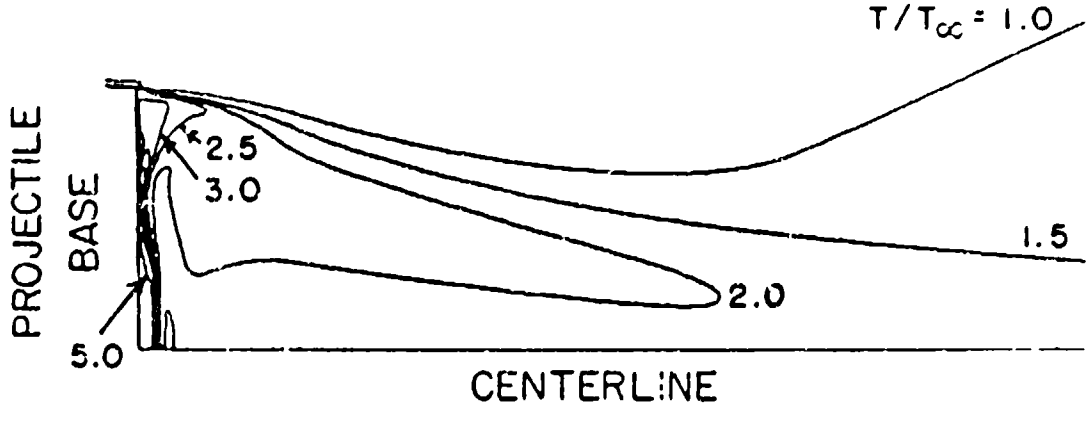

Figure 54. Temperature contours: hot air injection, $M_\infty = 2$, I = 0.0022, $T_\infty = 294$ K, $T_w = 294$ K, $T_{o,r} = 1533$ K

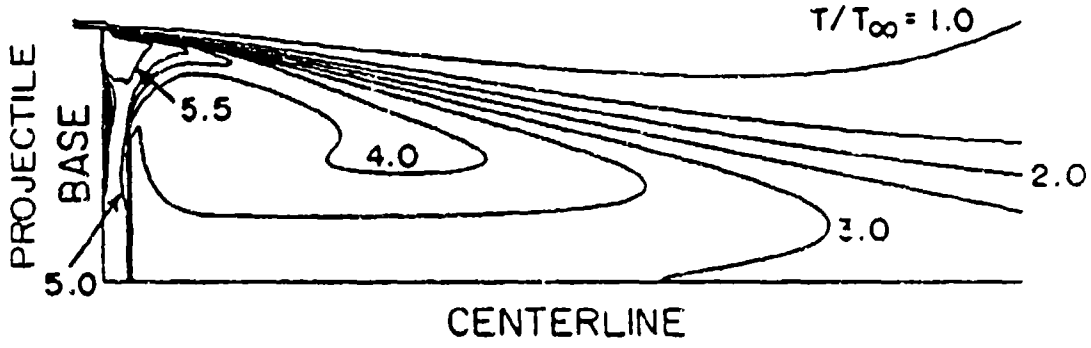

Figure 55. Temperature contours: H_2-CO injection, M_∞ = 2, I = 0.0022, T_∞ = 294 K, T_w = 294 K, T_{inj} = 1533 K

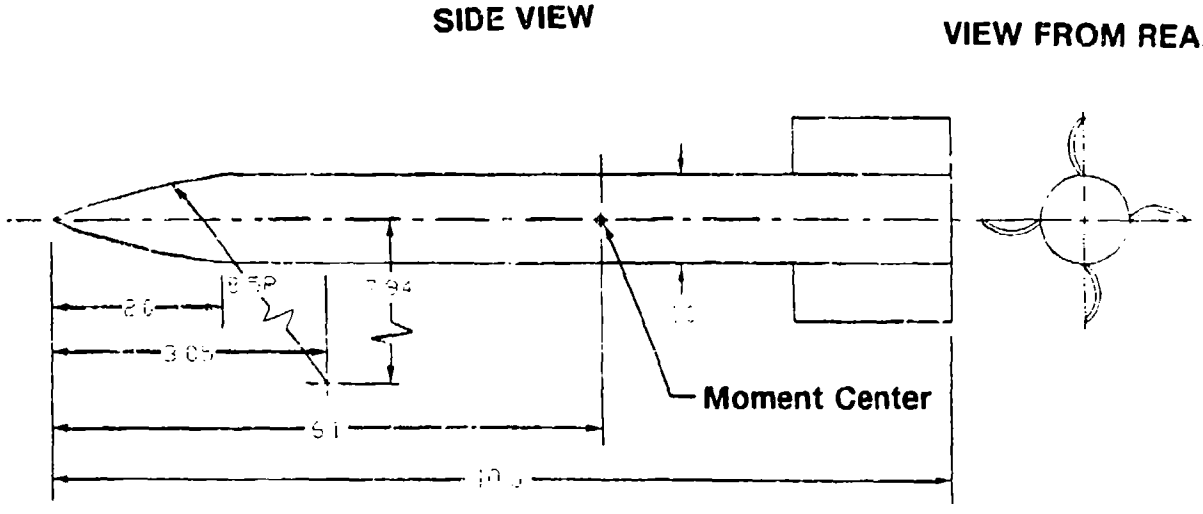

All Dimensions in Calibers
One Caliber - 10.16cm

Figure 56. Wrap-around fin projectile geometry

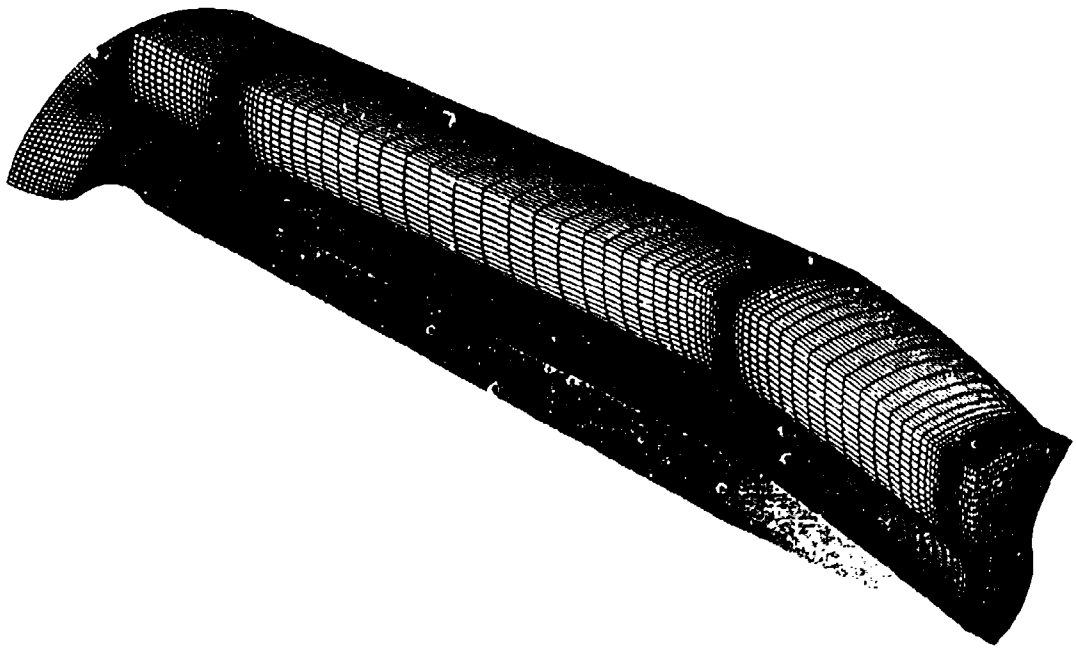

Figure 57. Wrap-around fin projectile grid

INTENTIONALLY LEFT BLANK.

10. REFERENCES

[1]Sturek, W. B., "Application of CFD to the Aerodynamics of Spinning Shell," AIAA Paper 84-0323, January 1984.

[2]Nietubicz, C. J. and Sturek, W. B., "Navier-Stokes Code Verification for Projectile Configurations at Supersonic and Transonic Velocities," AIAA Paper 88-1995, May 1988.

[3]Sahu, J. and Steger, J. L., "Numerical Simulation of Three Dimensional Transonic Flows," BRL-TR-2903, U.S. Army Ballistic Research Laboratory, Aberdeen Proving Ground, MD, March 1988. Also AIAA Paper No. 87-2293.

[4]Nietubicz, C. J., Pulliam, T. H., and Steger, J. L., "Numerical Solution of the Azimuthal-Invariant Thin-Layer Navier-Stokes Equations," AIAA Journal, Vol. 18, No. 12, 1980, pp. 1411-1412.

[5]Beam, R. and Warming, R. F., "An Implicit Factored Scheme for the Compressible Navier-Stokes Equations," AIAA Journal, Vol. 16, No. 4, 1978, pp. 393-402.

[6]Schiff, L. B. and Steger, J. L., "Numerical Simulation of Steady Supersonic Viscous Flow," AIAA Journal, Vol. 18, No. 12, 1980, pp. 1421-1430.

[7]Rai, M. M. and Chaussee, D. S., "New Implicit Boundary Procedure: Theory and Applications," AIAA Paper 83-0123, January 1983.

[8]Rai, M. M., Chaussee, D. S., and Rizk, Y. M., "Calculation of Viscous Supersonic Flows over Finned Bodies," AIAA Paper 83-1667, July 1983.

[9]Steger, J. L., Nietubicz, C. J., and Heavey, K. R., "A General Curvilinear Grid Generation Program for Projectile Configurations," BRL-MR-03142, U.S. Army Ballistic Research Laboratory, Aberdeen Proving Ground, MD, October 1981.

[10]Nietubicz, C. J., Heavey, K. R., and Steger, J. L., "Grid Generation Techniques for Projectile Configurations," Proceedings of the 1982 Army Numerical Analysis and Computers Conference, October 1982, ARO Report No. 82-3, pp. 99-121

[11]Ferry, E. N., Jr. and Nietubicz, C. J., "Interactive Hyperbolic Grid Generation for Projectile CFD," BRL-MR-3971, U.S. Army Ballistic Research Laboratory, Aberdeen Proving Ground, MD, May 1992.

[12]Baldwin, B. S. and Lomax, H., "Thin Layer Approximation and Algebraic Model for Separated Turbulent Flows," AIAA Paper 78-257, January 1978.

[13]Chow, W. L., "Improvement on Numerical Computation of the Thin-Layer Navier-Stokes Equation -- With Emphasis on the Turbulent Base Pressure of a Projectile in Transonic Flight Condition," University of Illinois Contract Report, Contract No. DAAG29-81-D-0100, Delivery Order 1713, November 1985.

[14]Sahu, J. and Danberg, J. E., "Navier-Stokes Computations of Transonic Flow with a Two Equation Model," AIAA Journal, Vol. 24, No. 11, 1986, pp. 1744-1751.

[15]Murphy, C. H., "Free Flight Motion of Symmetric Missiles," BRL Report No. 1216, U.S. Army Ballistic Research Laboratory, Aberdeen Proving Ground, MD, July 1963.

[16]Tobak, M., Schiff, L. B., and Peterson, V. L., "Aerodynamics of Bodies of Revolution in Coning Motion," AIAA Journal, Vol 7., No. 1, 1969, pp. 95-99.

[17]Weinacht, P., Sturek, W. B., and Schiff, L. B., "Navier-Stokes Predictions of Pitch Damping for Axisymmetric Shell Using Steady Coning Motion," AIAA Paper 91-2855, August 1991.

[18]Sahu, J., "Transonic Critical Aerodynamic Behavior," AIAA Journal, Vol. 28, No. 5, 1990, pp. 807-816. Also published as a BRL-TR-2962, U.S. Army Ballistic Research Laboratory, Aberdeen Proving Ground, MD, December 1988.

[19]Kayser L. D. and Whiton, F., "Surface Pressure Measurements on a Boattailed Projectile Shape at Transonic Speeds," BRL-MR-03161, U.S. Army Ballistic Research Laboratory, Aberdeen Proving Ground, MD, March 1982.

[20]Miller, M. C. and Molnar, J. W., "Wind Tunnel Measurements of the Magnus Induced Surface Pressures on a Spinning Artillery Projectile Model in the Transonic Speed Regime," CRDEC-TR-86081, Chemical Research, Development and Engineering Center, Aberdeen Proving Ground, MD, September 1986.

[21]Sahu, J., "Transonic Navier-Stokes Computations for a Spinning Body of Revolution," BRL-TR-3265, U.S. Army Ballistic Research Laboratory, Aberdeen Proving Ground, MD, September 1991.

[22]Platou, A. S. and Nielsen, G.I.T., "Some Aerodynamic Characteristics of the Artillery Projectile XM549," BRL-MR-2284, U.S. Army Ballistic Research Laboratory, Aberdeen Proving Ground, MD, April 1973.

[23]Herrin, J. L. and Dutton, J. C., "An Experimental Investigation of the Supersonic Axisymmetric Base Flow Behind a Cylindrical Afterbody," UICU 91-4004, University of Illinois at Urbana-Champaign, Urbana, IL, May 1991.

[24]Sahu, J., "Numerical Computations of Supersonic Base Flow with Special Emphasis on Turbulence Modeling," AIAA Paper 92-4352, August 1992.

[25]Nietubicz, C. J. and Sahu, J., "Navier-Stokes Computations of Base Bleed Projectiles," Base Bleed: First International Symposium on Special Topics in Chemical Propulsion, edited by K.K. Kuo and J.F. Fleming, Hemisphere Publishing Corporation, Washington, D.C., 1991, pp. 93-106.

[26]Danberg, J. E. and Nietubicz, C. J., "Predicted Flight Performance of Base-Bleed Projectiles," Journal of Spacecraft and Rockets, Vol. 29, No. 3, 1992, pp. 366-372.

[27]Weinacht, P. and Sturek, W. B., "Navier-Stokes Predictions of Static and Dynamic Aerodynamic Derivatives for High L/D Projectiles," Proceedings of the 66th AGARD Fluid Dynamics Panel Symposium on Missile Aerodynamics, Friedrichshafen, West Germany, April 1990.

[28]Weinacht, P. and Sturek, W. B., "Navier-Stokes Predictions of Pitch Damping for Finned Projectiles Using Steady Coning Motion," AIAA Paper 90-3088, August 1990.

[29]Celmins, I., "Aerodynamic Characteristics of Fin and Flare-Stabilized 25mm XM910 Prototypes," BRL-TR-2882, U.S. Army Ballistic Research Laboratory, Aberdeen Proving Ground, Maryland, December 1987.

[30]Weinacht, P., "Navier-Stokes Prediction of Pitch Damping for a Family of Flared Projectiles," AIAA Paper 91-3339-CP, September 1991.

[31]Danberg, J. E., Sigal, A., and Celmins, I., "Aerodynamic Characteristics of a Family of Cone-Cylinder-Flare Projectiles," Journal of Spacecraft and Rockets, Vol. 27, No. 4, 1990, pp. 355-360.

[32]Weinacht, P., "Aerodynamic Predictions for the Scorpion Parent Projectile Using a Navier-Stokes Approach," BRL-TR-3350, U.S. Army Ballistic Research Laboratory, Aberdeen Proving Ground, MD, June 1992.

[33]Sahu, J. and Nietubicz, C. J., "A Computational Study of Cylindrical Segments in the Wake of a Projectile," BRL-TR-3254, U.S. Army Ballistic Research Laboratory, Aberdeen Proving Ground, Maryland, August 1991.

[34]Weinacht, P., "Aerodynamic Predictions for Extending Projectile Designs," BRL-TR-3350, U.S. Army Ballistic Research Laboratory, Aberdeen Proving Ground, Maryland, June 1992.

[35]Sahu, J. and Nietubicz, C. J., "Three Dimensional Flow Calculations for a Projectile with Standard and Dome Bases," SAE Paper 89-2291, September 1989.

[36]Sahu, J., "A Computational Study of the Base Region Flow Field for the M865 Projectile," to be published as a U.S. Army Research Laboratory Report.

[37]Sturek, W. B., Kayser, L. D., and Weinacht, P., "Computational Study of Swept-Fin Aerodynamic Heating for the 105mm M774," ARBRL-MR-03315, U.S. Army Ballistic Research Laboratory, Aberdeen Proving Ground, MD, October 1983.

[38]Sturek, W. B., Dwyer, H. A., and Ferry, E. N., Jr., "Prediction of In-Bore and Aerodynamic Heating of KE Projectile Fins," BRL-MR-3852, U.S. Army Ballistic Research Laboratory, Aberdeen Proving Ground, MD, August 1990.

[39]Sturek, F. D., Sturek, W. B., and Ferry, E. N., Jr., "A Computational Study of the Effectiveness of Coating Materials for KE Projectile Fins Subjected to the Combined Effects of Inbore and Aerodynamic Heating," BRL-MR-3831, U.S. Army Ballistic Research Laboratory, Aberdeen Proving Ground, MD, April 1990.

[40]Giebling, H. J. and Buggeln, R. C., "Reacting Flow Models for Navier-Stokes Analysis of Projectile Base Combustion," AIAA Paper 91-2077, June 1991.

[41]Edge, H. L., "Computation of the Roll Moment Coefficient for a Projectile with Wrap-Around Fins," ARL-TR-23, U.S. Army Research Laboratory, Aberdeen Proving Ground, MD, December 1992.

[42]Benek, J. A., Buning, P. G., and Steger, J. L., "A 3-D Chimera Grid Embedding Technique," AIAA Paper No. 85-1523, 1985.

[43]Meakin, R. L. and Suhs, N., "Unsteady Aerodynamic Simulation of Multiple Bodies in Relative Motion," AIAA Paper 89-1996, 1989.

[44]Meakin, R. L., "Overset Grid Methods for Aerodynamic Simulation of Bodies in Relative Motion," Proceedings of the 8th Aircraft/Stores Compatibility Symposium, Ft. Walton Beach, FL, October 1990.

LIST OF SYMBOLS

a	=	speed of sound
CP	=	center of pressure for normal force
C_{Do}	=	zero yaw drag coefficient
C_{lo}	=	roll producing moment coefficient
C_{lp}	=	roll damping coefficient
C_m	=	pitching moment coefficient
C_{m_α}	=	$dC_m / d\alpha$, slope of normal force coefficient evaluated at $\alpha = 0$
$C_{m_q} + C_{m_{\dot{\alpha}}}$	=	pitch damping moment coefficient
C_N	=	normal force coefficient
C_{N_α}	=	slope of normal force coefficient
C_p	=	pressure coefficient $(p - p_\infty) / (\frac{1}{2}\rho_\infty u^2_\infty)$
C_Y	=	Magnus (side) force coefficient
d	=	local diameter of model
D	=	reference diameter of model
I	=	mass injection parameter $m / (\rho_\infty U_\infty A_b)$
L	=	reference length
m	=	mass flow rate
M	=	Mach number
P	=	pressure normalized by $\rho_\infty a^2_\infty$
PD / V	=	nondimensional spin rate
Re	=	Reynolds number
T	=	temperature
u	=	velocity component, x
v	=	velocity component, v

Greek Symbols

α	=	angle of attack
ρ	=	density

Subscripts

∞	=	free-stream conditions
b	=	base
w	=	body surface values
oinj	=	injected gas

No. of Copies	Organization
2	Administrator Defense Technical Info Center ATTN: DTIC-DDA Cameron Station Alexandria, VA 22304-6145
1	Commander U.S. Army Materiel Command ATTN: AMCAM 5001 Eisenhower Ave. Alexandria, VA 22333-0001
1	Director U.S. Army Research Laboratory ATTN: AMSRL-D 2800 Powder Mill Rd. Adelphi, MD 20783-1145
1	Director U.S. Army Research Laboratory ATTN: AMSRL-OP-CI-AD, Tech Publishing 2800 Powder Mill Rd. Adelphi, MD 20783-1145
2	Commander U.S. Army Armament Research, Development, and Engineering Center ATTN: SMCAR-IMI-I Picatinny Arsenal, NJ 07806-5000
2	Commander U.S. Army Armament Research, Development, and Engineering Center ATTN: SMCAR-TDC Picatinny Arsenal, NJ 07806-5000
1	Director Benet Weapons Laboratory U.S. Army Armament Research, Development, and Engineering Center ATTN: SMCAR-CCB-TL Watervliet, NY 12189-4050
(Unclass. only)1	Commander U.S. Army Rock Island Arsenal ATTN: SMCRI-IMC-RT/Technical Library Rock Island, IL 61299-5000
1	Director U.S. Army Aviation Research and Technology Activity ATTN: SAVRT-R (Library) M/S 219-3 Ames Research Center Moffett Field, CA 94035-1000

No. of Copies	Organization
1	Commander U.S. Army Missile Command ATTN: AMSMI-RD-CS-R (DOC) Redstone Arsenal, AL 35898-5010
1	Commander U.S. Army Tank-Automotive Command ATTN: ASQNC-TAC-DIT (Technical Information Center) Warren, MI 48397-5000
1	Director U.S. Army TRADOC Analysis Command ATTN: ATRC-WSR White Sands Missile Range, NM 88002-5502
1	Commandant U.S. Army Field Artillery Schoo! ATTN: ATSF-CSI Ft. Sill, OK 73503-5000
(Class. only)1	Commandant U.S. Army Infantry School ATTN: ATSH-CD (Security Mgr.) Fort Benning, GA 31905-5660
(Unclass. only)1	Commandant U.S. Army Infantry School ATTN: ATSH-CD-CSO-OR Fort Benning, GA 31905-5660
1	WL/MNOI Eglin AFB, FL 32542-5000
	Aberdeen Proving Ground
2	Dir, USAMSAA ATTN: AMXSY-D AMXSY-MP, H. Cohen
1	Cdr, USATECOM ATTN: AMSTE-TC
1	Dir, ERDEC ATTN: SCBRD-RT
1	Cdr, CBDA ATTN: AMSCB-CI
1	Dir, USARL ATTN: AMSRL-SL-I
10	Dir, USARL ATTN: AMSRL-OP-CI-B (Tech Lib)

No. of Copies Organization

4 Commander
U.S. Army Armament Research, Development and Engineering Center
ATTN: SMCAR-AET-A,
R. Kline
H. Hudgins
S. Kahn
J. Grau
Picatinny Arsenal, NJ 07806-5001

1 Commander
U.S. Army Missile Command
ATTN: AMSMI-RD-SS-AT,
B. Walker
Redstone Arsenal, AL 35898-5010

1 Commander
U.S. Naval Surface Weapons Center
ATTN: Dr. F. Moore
Dahlgren, VA 22448

3 Commander
Naval Surface Weapons Center
ATTN: Code R44,
Dr. F. Priolo
Dr. A. Wardlaw
K24, B402-12,
Dr. W. Yanta
White Oak Laboratory
Silver Spring, MD 20903-5000

1 Air Force Armament Laboratory
Air Force Systems Command
ATTN: AFATL/FXA, Dr. L.B. Simpson
Eglin AFB, FL 32542-5434

1 USAF Wright Aeronautical Laboratories
ATTN: AFWAL/FIMG,
Dr. J. Shang
WPAFB, OH 45433-6553

3 Director
National Aeronautics and Space Administration
Langley Research Center
ATTN: Tech Library
Dr. M. J. Hemsch
Dr. J. South
Langley Station
Hampton, VA 23665

No. of Copies Organization

3 Director
National Aeronautics and Space Administration
Ames Research Center
ATTN: MS-227-8, L. Schiff
MS-258-1,
T. Holst
D. Chaussee
Moffett Field, CA 94035

1 Massachusetts Institute of Technology
ATTN: Technical Library
77 Massachusetts Avenue
Cambridge, MA 02139

3 Sandia National Laboratories
ATTN: Dr. Daniel Barnette
Dr. W. Oberkampf
Dr. F. Blottner
Division 1554
P.O. Box 5800
Albuquerque, NM 87185

2 VRA Inc.
ATTN: Dr. C. Lewis
Dr. B.A. Bhutta
P.O. Box 50
Blacksburg, VA 24060

1 Science Applications, Inc.
Computational Fluid Dynamics Division
ATTN: Dr. D.W. Hall
994 Old Eagle School Road
Suite 1018
Wayne, PA 19087

1 Alliant Techsystems, Inc.
ATTN: MN48-3700, Dr. R. Buretta
7225 Northland Drive
Brooklyn Park, MN 55428

No. of Copies Organization

1 McDonnell Douglas Missile Systems Co.
ATTN: F. McCotter
Mailcode 308-4249
P.O. Box 516
St. Louis, MO 63166-0516

2 Institute for Advanced Technology
ATTN: Dr. T. Kiehne
Dr. W.G. Reineke
4030-2 W. Baker Lane
Austin, TX 78759

1 University of California, Davis
Department of Mechanical Engineering
ATTN: Prof. H. A. Dwyer
Davis, CA 95616

1 University of Maryland
Department of Aerospace Engineering
ATTN: Dr. J. D. Anderson, Jr.
College Park, MD 20742

1 University of Texas
Department of Aerospace Engineering
and Engineering Mechanics
ATTN: Dr. D. S. Dolling
Austin, TX 78712-1055

1 University of Florida
Department of Engineering Sciences
College of Engineering
ATTN: Prof. C. C. Hsu
Gainesville, FL 32611

1 Pennsylvania State University
Department of Mechanical Engineering
ATTN: Dr. Kenneth Kuo
University Park, PA 16802

1 Florida Atlantic University
Department of Mechanical Engineering
ATTN: Dr. W. L. Chow
Boca Raton, FL 33431

1 North Carolina State University
Department of Mechanical and Aerospace
Engineering
ATTN: Prof. D.S. McRae
Box 7910
Raleigh, NC 27695-7910

No. of Copies Organization

1 University of Illinois at
Urbana-Champaign
Department of Mechanical and Industrial
Engineering
ATTN: Prof. A.L. Addy
114 Mechanical Engineering Building
1206 West Green Street
Urbana, IL 61801

1 Georgia Institute of Technology
School of Aerospace Engineering
ATTN: Dr. Warren C. Strahle
Atlanta, GA 30332

2 Scientific Research Associates
ATTN: Dr. Howard Gibeling
Dr. Richard Buggeln
50 Nye Road
P.O. Box 1058
Glastonbury. CT 06033

1 AEDC
Calspan Field Service
ATTN: Dr. John Benek
MS 600
Tullahoma, TN 37389

1 McDonnell Douglas Corporation
Dept 222 Bldg 110 Lev 1 RM/PT 151
Mail Code 5
ATTN: Dr. Thomas P. Gielda
P.O. Box 516
Saint Louis, MO 63166-0516

1 Visual Computing
ATTN: Jeffrey Q. Cordova
883 N. Shoreline Blvd.
Suite B210
Mountain View, CA 94043

1 MDA Engineering, Inc.
ATTN: John P. Steinbrenner
500 E. Border St.
Suite 401
Arlington, TX 76010

INTENTIONALLY LEFT BLANK

USER EVALUATION SHEET/CHANGE OF ADDRESS

This Laboratory undertakes a continuing effort to improve the quality of the reports it publishes. Your comments/answers to the items/questions below will aid us in our efforts.

1. ARL Report Number ARL-TR-22 Date of Report December 1992

2. Date Report Received _____

3. Does this report satisfy a need? (Comment on purpose, related project, or other area of interest for which the report will be used.) _____

4. Specifically, how is the report being used? (Information source, design data, procedure, source of ideas, etc.) _____

5. Has the information in this report led to any quantitative savings as far as man-hours or dollars saved, operating costs avoided, or efficiencies achieved, etc? If so, please elaborate. _____

6. General Comments. What do you think should be changed to improve future reports? (Indicate changes to organization, technical content, format, etc.) _____

CURRENT ADDRESS

_____
Organization

_____
Name

_____
Street or P.O. Box No.

_____
City, State, Zip Code

7. If indicating a Change of Address or Address Correction, please provide the Current or Correct address above and the Old or Incorrect address below.

OLD ADDRESS

_____
Organization

_____
Name

_____
Street or P.O. Box No.

_____
City, State, Zip Code

(Remove this sheet, fold as indicated, staple or tape closed, and mail.)